JCI The Journal of Clinical Investigation

Dectin-2-induced CCL2 production in tissue-resident macrophages ignites cardiac arteritis

Chie Miyabe, … , Tamihiro Kawakami, Andrew D. Luster

J Clin Invest. 2019. https://doi.org/10.1172/JCI123778.

Research In-Press Preview Immunology Inflammation

Graphical abstract

Dectin-2-induced CCL2 production in tissue-resident macrophages ignites cardiac arteritis

Chie Miyabe[1], Yoshishige Miyabe[1], Laura Moreno[1], Jeffrey Lian[1], Rod A. Rahimi[1], Noriko N. Miura[2], Naohito Ohno[2], Yoichiro Iwakura[3], Tamihiro Kawakami[4] and Andrew D. Luster[1]

[1]Center for Immunology and Inflammatory Diseases, Division of Rheumatology, Allergy and Immunology, Massachusetts General Hospital, Harvard Medical School, Boston, Massachusetts, USA.

[2]Tokyo University of Pharmacy and Life Science, Tokyo, Japan.

[3]Center for Animal Disease Models, Research Institute for Biomedical Sciences, Tokyo University of Science, Chiba, Japan.

[4]Department of Dermatology, Tohoku Medical and Pharmaceutical University, Sendai, Japan.

Correspondence should be addressed to:
Andrew D. Luster, M.D., Ph.D.
Center for Immunology and Inflammatory Diseases
Division of Rheumatology, Allergy and Immunology
Massachusetts General Hospital
Building 149-8.304, 13th Street
Charlestown, MA 02129
Email aluster@mgh.harvard.edu
Voice 617-726-5710
FAX 617-726-5651

Conflict of interest statement: The authors have declared that no conflict of interest exists.

Abstract

Environmental triggers, including those from pathogens, are thought to play an important role in triggering autoimmune diseases, such as vasculitis, in genetically susceptible individuals. The mechanism by which activation of the innate immune system contributes to vessel-specific autoimmunity in vasculitis is not known. Systemic administration of *Candida albicans* water-soluble extract (CAWS) induces vasculitis in the aortic root and coronary arteries of mice that mimics human Kawasaki disease. We found that Dectin-2 signaling in macrophages resident in the aortic root of the heart induced early CCL2 production and the initial recruitment of $CCR2^{+}$ inflammatory monocytes (iMo) into the aortic root and coronary arteries. iMo differentiated into monocyte-derived dendritic cells (Mo-DC) in the vessel wall and were induced to release IL-1β in a Dectin-2-Syk-NLRP3 inflammasome dependent pathway. IL-1β then activated cardiac endothelial cells to express CXCL1 and CCL2 and adhesion molecules that induced neutrophil and further iMo recruitment and accumulation in the aortic root and coronary arteries. Our findings demonstrate that Dectin-2-mediated induction of CCL2 production by macrophages resident in the aortic root and coronary arteries initiates vascular inflammation in a model of Kawasaki disease, suggesting an important role for the innate immune system in initiating vasculitis.

Introduction

Kawasaki disease (KD), first described as an acute febrile mucocutaneous lymph node syndrome in 1967 (1), is the most common systemic vasculitis of children and infants. KD is recognized as the leading cause of acquired heart disease among children in developed countries (2). KD primarily involves the coronary arteries, but vasculitis can occur at various sites throughout the body (3). Coronary artery abnormalities, including dilatation and aneurysms, are the most serious complications that develop in ~25% of untreated cases, which can lead to myocardial ischemia, infarction, and death (4). High-dose intravenous immunoglobulin (IVIG) therapy reduces the risk of coronary artery lesions (5), however, approximately 10-15% of the KD patients do not respond to IVIG, and appropriate treatment for these cases is not established (6). Therefore, understanding the pathogenesis of KD is critical for the rationale design of improved therapies for preventing the cardiac complications of KD.

Although the etiology of KD is not known, an infectious agent has been suspected due to the reported seasonal peak during winter and spring seasons (7). Moreover, a number of studies have linked KD with exposure to freshly cleaned carpets, habitation near a body of water, and humidifier use. Various bacterial and viral agents have been implicated as potential causes of KD, but no proof has emerged to incriminate a single pathogen (8). In addition, there is also growing evidence supporting genetic contributions to the susceptibility to KD (9). These findings suggest that infectious triggers in genetically susceptible individuals likely play an important role in the development of KD vasculitis.

Because of inherent difficulties in studying human patients with vasculitis, animal models have served as important tools for improving our understanding of the basic mechanisms underlying the pathogenesis of vasculitis (10). Over the last few decades, several murine models of KD have been developed that share pathological features with the human disease, including the *Candida albicans* water-soluble extract (CAWS)-induced vasculitis model (11, 12), the *Lactobacillus casei* cell wall extract (LCWE)-induced vasculitis model (13), and the NOD1 ligand-induced vasculitis model (14). Although animal models are not identical to human disease and it is not established that *Candida* causes KD, previous studies have suggested that exposure to wind-borne *Candida species* might be one trigger for KD (15-17). In addition, it has been reported that anti-*Candida* cell wall beta-glucan serum antibody titers are higher in KD patients compared to normal controls (18). These reports suggest potential physiological relevance for the CAWS-induced vasculitis model. Interestingly, all of these models have in common strong innate immune system activation by Pathogen-Associated Molecular Patterns (PAMPs). Pattern recognition receptors (PRR), including TLRs, retinoic acid-inducible gene-I-like receptors (RLR), and C-type lectin receptors (CLR), recognize PAMPs and initiate the innate immune response (19).

Here we explored the mechanism by which the initiation of an innate immune response leads to vasculitis using the CAWS-induced murine model of vasculitis. CAWS consists of *Candida albican's* cell wall, including α-mannan and β-glucan (20). Both CLRs and TLRs play a role in *Candida* recognition. Among the CLRs, Dectin-1 recognizes β-glucans whereas Dectin-2 recognizes α-mannans in fungal cell walls (21, 22). Both Dectin-1 and Dectin-2 are glycosylated type II transmembrane proteins, which are mainly expressed on

myeloid cells, and induce cytokines and reactive oxygen species to protect hosts from fungal infection through activation of a spleen tyrosine kinase (Syk)-CARD9-NF-κB pathway in DCs and macrophages (23). Whereas Dectin-1 has a tyrosine-based activation motif (ITAM)-like motif (hemITAM) in its intracellular region, Dectin-2 associates with an ITAM-containing Fc receptor (FcR) γ signaling chain. Among the TLRs, TLR2 recognizes phospholipomannan while TLR4 recognizes O-linked mannosyl residues of the *Candida* cell wall, which are involved in the induction of host immune response to *Candida* (24).

Here we describe a novel mechanism whereby the innate immune response ignites autoimmune vessel specific inflammation. We show that CAWS antigen is preferentially deposited in the adventitia of the aortic root where is recognized by Dectin-2 expressed on resident macrophages in the adventitia. Dectin-2-activated resident macrophages produce CCL2, which induces the recruitment of inflammatory monocytes (iMo) into the aortic root, which the initial step required for the induction of aortic root and coronary artery vasculitis resembling KD. iMo differentiate into monocyte-derived dendritic cells (Mo-DC) and produce IL-1β via a Dectin-2-NF-kB-NAPL3 inflammasome pathway, resulting in chemokine production in the inflamed vessel amplifying neutrophil and iMo recruitment.

Results

CAWS induces inflammatory cell recruitment into the aortic root area.

CAWS induces marked inflammatory cell infiltration into the aortic root area **(Figure 1A)**. To clarify the temporal and spacial distribution of inflammatory cell infiltration into the heart during the development of CAWS-induced arteritis, we analyzed the number of inflammatory cells in coronal section of the entire heart before and on days 1, 7 and 28 after beginning CAWS injection on day 0 by IHC using Ly6G/Ly6C to stain neutrophil and iMo and F4/80 to stain resident macrophage **(Fig. 1B and C)**. The vast majority of Ly6G/Ly6C$^+$ and F4/80$^+$ cells accumulated in the aortic root area during the development of vasculitis peaking on day 28 with a small number of Ly6G/Ly6C$^+$ cells transiently observed in the myocardium on day 1 **(Supplemental Fig. 1)**. These results suggest that CAWS injection induces inflammatory cell recruitment mainly into the aortic root area as has been previously reported (11, 12, 25). These results indicate that while we have used the entire heart for subsequent FACS analysis, it is presumed that the majorty of inflammatory cells detected by flow cytometry were from the aortic root area of the heart.

To define the initiating events promoting coronary arteritis, we performed a detailed kinetic analysis of myeloid cell subset recruited into the heart after 5 daily intraperitoneal injections of CAWS into C57BL/6 WT mice. Whole heart cell suspensions were obtained after enzyme digestion and analyzed by flow cytometry on days 0, 1, 2, 4, 7 and 28 after the first dose of CAWS. After gating on live CD45$^+$ cells and excluding cells expressing CD90.2, CD19 and NK1.1 to remove T cells, B cells and NK cells, a sequential gating strategy was employed based on the differential expression of CD11b, Ly6G, CD64, MerTK, Ly6C,

MHCll and CD11c to define myeloid cell subsets (26, 27). This allowed the identification of cardiac macrophages ($CD64^+MerTK^+$), neutrophils ($CD11b^+Ly6G^+$), cDC ($CD11c^+MHCll^+$), $Ly6C^{hi}$ monocytes ($Ly6C^{hi}MHCll^-$) and Mo-DC ($Ly6C^{lo/-}MHCll^+$) in the heart **(Fig. 1D)**. Using this gating strategy, we found that there was a burst of $Ly6C^{hi}$ monocyte and neutrophil infiltration on day 1 (initial phase) after CAWS injection followed by a decrease by day 2. Thereafter the number of Mo-DC started to increase on day 7 (middle phase) followed by a massive influx of neutrophils on day 28 (late phase) **(Fig. 1E)**.

To determine the contribution of circulating cells to the increase in immune cells recovered from the heart following CAWS injection, a parabiosis experiment was performed. $CD45.1^+$ and $CD45.2^+$ mice were co-joined for 2 weeks to allow for the establishment of a joined circulation followed by the injection of CAWS into both parabionts **(Fig. 1F)**. Mice were harvested two weeks after the initial CAWS injection and the ratio of $CD45^+$ cells derived from the host and partner was ~60:40 in the heart, which was the same ratio as observed in blood. This demonstrates that the inflammatory cells found in the heart after CAWS injection were recruited from the circulation **(Fig. 1G)**. The chimerism of each myeloid cell type was also ~60:40 in the heart **(Fig. 1, H and I)**. These data show that the immune cells within the inflamed cardiac tissues were mainly recruited from the blood.

CCL2 is induced in heart and promotes $CCR2^+$ monocyte recruitment.

Given the rapid infiltration of innate immune cells after CAWS injection, we next examined chemokine expression in the entire heart during the development of arteritis. Chemokine mRNA levels in the heart were induced differently over time following CAWS injection

(Supplemental Fig. 2). At day 1 after the 1st CAWS injection, several monocyte-attracting chemokines, including the CCR2 ligands CCL2, CCL7, and CCL12, were induced. CCR2 ligands peaked at day 1 while neutrophil-attracting chemokines, such as the CXCR2 ligands CXCL1 and CXCL2, peaked at day 28. These data suggest that during the course of CAWS-induced coronary inflammation, monocytes expressing CCR2 are recruited into the heart at early time points, while CXCR2-expressing PMNs are recruited into the heart at later time points. A detailed time course of CCL2 expression demonstrated a transient increase at day 1 after CAWS injection **(Fig. 2A)**. Remarkably, CCL2 was exclusively expressed in the heart at day 1 post CAWS injection, and was not detected in other organs at this time point, including lung, spleen, kidney and liver **(Fig. 2B)**. Other CCR2 ligands, such as CCL7 and CCL12, were also exclusively induced in the heart one day following CAWS injection, while other chemokines tested were not specifically induced in the heart **(Supplemental Fig. 3)**.

To determine the role of CCR2 in monocyte trafficking from the blood into the heart, we performed adoptive transfer competitive trafficking experiments using WT and *Ccr2*$^{-/-}$ monocytes. WT monocytes were purified from *LysM*-GFP mice where expression of the green fluorescent protein (GFP) is driven by the lysozyme M promoter, resulting in GFP positive neutrophils and monocytes (28). *Ccr2*$^{-/-}$ monocytes were purified from CCR2-red fluorescent protein knock-in mice, which lack CCR2 in *Ccr2*$^{RFP/RFP}$ homozygous mice (29). Equal numbers of *Ccr2*$^{+/+}$GFP^{+} and *Ccr2*$^{-/-}$RFP^{+} monocytes were isolated from the bone marrow of naïve mice, mixed 1:1 and intravenously injected into WT mice along with intraperitoneal CAWS injection. 20h after adoptive transfer, tissues were harvested and

analyzed for the presence of the *Ccr2*$^{+/+}$GFP^{+} and *Ccr2*$^{-/-}$RFP^{+} cells **(Fig. 2C)**. The ratio of *Ccr2*$^{+/+}$ and *Ccr2*$^{-/-}$monocytes in the heart was skewed towards *Ccr2*$^{+/+}$ monocytes at ~3:1 ratio while *Ccr2*$^{+/+}$ and *Ccr2*$^{-/-}$monocytes was found in the blood in a 1:1 ratio **(Fig. 2, D and E)**. We also tracked the transferred WT GFP^{+} bone marrow-derived monocytes (BMDM) on day 7 after CAWS injection **(Fig. 2F)**. This revealed that the transferred monocytes not only migrated into the heart but also differentiated into CD11c^{+}MHC-II^{+} Mo-DCs in the heart, which we found began to accumulate in the aortic root of the heart on day 7 **(Fig 1B)**. GFP^{+} cells in the heart showed increased expression of CD11c, MHC-II, CD172α and CD24, and decreased Ly6C expression, compared to the expression of these markers on these cells pretransfer **(Fig. 2, G and H)**, which is consistent with the transferred monocytes differentiating into Mo-DCs.

Given the importance of the CCL2/CCR2 pathway in early monocyte recruitment into the heart, we evaluated the vasculitis scores at day 28 in *Ccr2*$^{+/+}$ and *Ccr2*$^{-/-}$ mice. Notably, *Ccr2*$^{-/-}$ mice were totally protected from development of vasculitis **(Fig. 2, I and J)**. These results demonstrate that CAWS induced the CCR2-dependent recruitment of iMo into the heart in the early phase of cardiac inflammation and this process was necessary for induction of vasculitis.

Cardiac resident macrophages are the main source of CCL2 in the early phase of vasculitis. Given the specific induction of CCL2 in the heart on day 1 after CAWS injection, we sought to identify the cellular source of CCL2 production using *Ccl2-RFP*^{flox} mice, which report the cellular expression of the CCL2 protein (30). As shown by flow

cytometric analysis of the entire heart obtained from *Ccl2-RFP^{flox}* mice, CCL2 was expressed by heart cells at 6h and became prominent at 18h after CAWS injection (**Fig. 3A**). To determine whether cardiac stromal cells or leukocytes are producing CCL2, we compared CCL2 expression in four cell subsets in the heart: cardiac leukocytes ($CD45^+CD31^-$), endothelial cells ($CD45^-CD31^+$), fibroblasts ($CD45^-CD31^-$ $gp38^+$), and other stromal cells ($CD45^-CD31^-$ $gp38^-$) as previously described (25) **(Fig. 3A)**. Strikingly, leukocytes were the most abundant CCL2 producers at both 6h and 18h after CAWS injection with minor production by fibroblasts **(Fig. 3B)**. Among the leukocyte population, $CD64^+MerTK^+$ cardiac macrophages preferentially expressed CCL2 on day 1 after CAWS injection compared to other cell types **(Fig. 3C)**. We further characterized cardiac macrophages in the enitre heart on day 1 following CAWS injection by flow cytometry **(Supplementary Fig. 4)**. Cardiac macrophages uniformly expressed high levels of CD11b and F4/80 and CD11c at lower levels. A subpopulation of cardiac macrophages also expressed MHC-II and Dectin-2 but cardiac macrophages did not express CCR2 or Ly6C. These results suggest that cardiac resident macrophages are the major source of early CCL2 production in the heart following CAWS injection.

CCL2 is produced by $CD11b^+$Dectin-2^+ resident cardiac macrophages in the adventitia of the aortic root and coronary vessels. To visualize the location of CCL2-producing cells, we histologically analyzed heart tissue from *Ccl2-RFP^{flox}* mice on day 1 after CAWS injection and detected CCL2 protein expression in adventia of the aortic root and coronary arteries **(Fig. 4A-D).** While there was autofluorescence from cardiac myocytes, we could identify CCL2 protein expression associated with $CD11b^+$ and Dectin-2^+ cells, as well as occasional associated with $CD11c^+$ cells, but not with $Ly6G^+$ neutrophils, confirming that

CD11b$^+$ Dectin-2$^+$ cardiac macrophages were the main source of CCL2 on day 1. To determine the pattern of CCL2 expression in macrophages in the aortic root area and in the myocardium, we injected CAWS into *Ccl2-RFP$^{fl/fl}$* reporter mice and harvested the heart on day 1 for immunofluorescence analysis following staining for CD11b. CCL2 was preferentially produced by CD11b$^+$ cells in the aortic root area compared to the myocardium **(Supplemental Fig. 5)**. Although we have detected a number of CD11b$^+$ in myocardium on day 1, most of the CD11b$^+$ cells did not express CCL2.

CAWS components are delivered to the adventitia of the aortic root. Our results suggest that CCL2 was expressed exclusively in the heart one day following CAWS injection, and that the main source of CCL2 were cardiac macrophages. We next examined why and how cardiac macrophages are activated following CAWS injected into the peritoneal cavity. We first hypothesized that Dectin-2 expression might be higher in cardiac macrophages compared to macrophages from different organs, making them more sensitive to CAWS stimulaiton. However, qPCR analysis of sorted macrophages isolated for various organs of naïve mice indicated that Dectin-2 expression was not higher in cardiac macrophages compared to other organs (data not shown). Then we next asked if CAWS is delivered to the site of future inflammation in heart and thereby directly inducing macrophage activation. To this end, we performed immunofluorescent staining for CAWS using an antibody that reacts with proteins in the soluble *Candida albicans* extract **(Fig. 5A-C)**. Intriguingly, *Candida* components (green) were detected on day 1 in the arotic root and were associated and with CD11b$^+$ cells (red) **(Fig. 5B)**. In contrast, *Candida* particle was barely detectable in other organs, such as the lung, spleen, liver and kidney, even though CD11b$^+$ cells were present in these tissues **(Fig. 5C)**. Notably, *Candida* particles were not

detected in the myocardium on day 1 following CAWS injection **(Fig. 5 A and C)**. These results suggest that the preferential deposition CAWS antigen in the adventitia of the aortic root, which is rich in vasa vasorum, and includes the ostium of the coronary arteries, determines the cardiac vessel specific inflammation in this model.

Dectin-2 is required for CAWS-induced CCL2 production and development of arteritis. Given the role of Dectin-2 in recognition of mannans and the expression of this PRR on cardiac macrophages, we sought to define the role of Dectin-2^{+} cardiac macrophages for CCL2 production after CAWS. As cardiac macrophages express F4/80 (**Supplementary Fig. 4)**, we isolated F4/80^{+} cells from single cell suspension of naïve hearts using magnetic-activated cell sorting and then stimulated these cells with CAWS. CCL2 production was induced by CAWS in F4/80^{+} cardiac macrophages derived from WT mice but not from *Dectin-$2^{-/-}$* mice (**Fig. 6A**). Furthermore, CCL2 mRNA levels in heart tissue on day 1 following CAWS injection was markedly reduced in *Dectin-$2^{-/-}$* mice compared to WT mice (**Fig. 6B**). As cardiac fibroblasts also produced CCL2 after CAWS injection **(Fig. 3B)**, we determined whether CAWS was also capable of directly stimulating CCL2 production in primary cardiac fibroblasts in vitro. Cardiac fibroblasts did not produce CCL2 mRNA or protein in response to CAWS stimulation in vitro; however, IL-1β, TNFα and LPS were able to induce CCL2 mRNA and protein in cardiac fibroblasts **(Supplemental Fig. 6)**. While cardiac fibroblasts also contribute to CCL2 production in the heart, our results suggest they are not responding directly to CAWS but are presumably responding to other endogenous mediators released in the heart tissue in response to CAWS.

In addition to the CLRs Dectin-1 and Dectin-2, TLR2 and TLR4 have also been reported to recognize *Candida* PAMPs and contribute to *Candida* immunity (31). To determine which PRR is crucial for CAWS recognition and vasculitis induction, groups of *Tlr4*$^{-/-}$, *Tlr2* $^{-/-}$, *Dectin-1* $^{-/-}$ and *Dectin-2*$^{-/-}$ mice were injected with CAWS and vasculitis was assessed histologically. *Dectin-2* $^{-/-}$ mice were completely protected from vasculitis, while *Tlr4*$^{-/-}$, *Tlr2* $^{-/-}$ and *Dectin-1* $^{-/-}$ mice were only partially protected from vasculitis compared to WT mice (**Fig. 6, C and D**). These results indicate that Dectin-2, which recognizes the α-mannans on fungal hyphae, is a critical PRR for CAWS-induced vasculitis. Dectin-2 signals through CARD9 and Syk, resulting in NF-κB activation (23). The FcRγ chain is required for the surface expression and signaling of Dectin-2. Consistent with our *Dectin-2*$^{-/-}$ results, *FcγR*$^{-/-}$ *and Card9*$^{-/-}$ mice were also completely protected from CAWS-induced vasculitis (**Fig. 6E)**. As a *Dectin-2*$^{fl/fl}$ strain was not available, we alternatively assessed the contribution of Syk-dependent pathways directly in CD11c^{+} cells during the development of vasculitis. We crossed Syk$^{fl/fl}$ mice (32) with CD11c-Cre mice (33) to generate a CD11cΔSyk strain that specifically lacks Syk in CD11c expressing cells. Notably, CD11cΔSyk mice were completely protected from vasculitis compared to littermate controls (CD11cCre^{-}Syk$^{fl/fl}$) (**Fig. 6F**). One day after CAWS injection, CCL2 mRNA transcripts in the heart were markedly lower in CD11cΔSyk mice compared to control mice, implying a contribution of heart CD11c^{+} cells (possibly CD11c^{+} cardiac macrophages) in the production of CCL2 in response to CAWS (**Fig. 6G**).

Dectin-2-dependent production of IL-1β from CD11c^{+} cells is required for CAWS-induced arteritis. To examine the key cytokines in CAWS-induced arteritis we performed

qPCR analysis on RNA isolated from heart tissue on day 28 post CAWS treatment. IL-1β was highly expressed in the heart following CAWS treatment compared to other pro-inflammatory cytokines, including IL-6, TNF-α and IL-1α **(Fig. 7A)**. We then examined the role of IL-1α/β in the development of arteritis using *IL1a*$^{-/-}$*IL1b*$^{-/-}$ mice. Remarkably, *IL1a*$^{-/-}$ *IL1b*$^{-/-}$ mice were completely resistant to CAWS-induced arteritis **(Fig. 7B)**. Next, we generated bone marrow chimeric (BMC) mice to address whether IL-1α/β are required in hematopoietic cells or radioresistant-resident cells for arteritis development. After bone marrow engraftment, chimeric mice were subjected to CAWS injection and vasculitis scores were evaluated on day 28 (**Fig. 7C**). BMC mice that had WT bone marrow transplanted into (→) WT recipient mice were susceptible to arteritis. In contrast, *IL1a*$^{-/-}$*IL1b*$^{-/-}$→*IL1a*$^{-/-}$*IL1b*$^{-/-}$ controls were resistant to arteritis as were *IL1a*$^{-/-}$*IL1b*$^{-/-}$→ WT BMC. However, WT →*IL1a*$^{-/-}$*IL1b*$^{-/-}$ BMC developed arteritis comparable to WT → WT controls (**Fig. 7D**). These results demonstrate that IL-1α/β expression in radiosensitive cells is necessary and sufficient for arteritis, whereas IL-1α/β expression in radioresistant cells does not contribute to the development of arteritis.

To further identify the cellular source of IL-1β, we utilized *pIL1β-DsRed* transgenic mice expressing the Discosoma red fluorescent protein (DsRed) gene under the control of the IL-1β promoter (34). We analyzed DsRed expressing leukocyte subsets in the heart during the course of arteritis using the gating strategy described in Supplemental Fig. 7. Distribution of IL-1β-producing DsRed^{+} cells showed that following CAWS injection, IL-1β was actively transcribed in neutrophils on day 1 (early phase) followed by Mo-DC on day 7 (middle phase) and then was abundantly produced in neutrophils on day 28 (late phase) **(Fig. 7E)**.

To determine if Dectin-2 was necessary for IL-1β production in the heart, we evaluated IL-1β expression in WT and *Dectin-2*$^{-/-}$ hearts on days 7 and 28 after CAWS injection. IL-1β mRNA levels were markedly reduced in *Dectin-2*$^{-/-}$ hearts compared to WT hearts on days 7 and 28 after CAWS injection **(Fig. 7F)**. Similarly, IL-1β mRNA levels in CD11cΔSyk hearts were significantly reduced compared to control hearts on day 7 and 28 after CAWS injection **(Fig. 7G)**. These results indicate that both Dectin-2 and Syk signaling in CD11c^{+} cells are required for IL-1β expression in the heart after CAWS injection.

CAWS activates the NLRP3 inflammasome and promotes IL-1β production via Dectin-2. Translocation of cytoplasmic NF-κB p65 to the nucleus is a key step in activation of the NF-κB pathway. To determine whether Dectin-2 was required for CAWS-induced activation of the NF-κB pathway in BMDCs, NF-κB nuclear translocation was assessed by immunofluorescence staining. Sixty mins following stimulation of BMDC with CAWS, or LPS as a positive control, NF-κB p65 (red) was detected in the cell nucleus (blue). CAWS induced NF-κB p65 translocation from the cytoplasm to the nucleus in WT BMDCs, but this translocation was largely absent in *Dectin-2* $^{-/-}$ BMDCs (**Fig. 8A**). NF-κB nuclear translocation was assessed and quantified as the percentage of p65 nuclei-positively stained cells to total cells (**Fig. 8B**). Similar results were obtained from *Dectin-2* $^{-/-}$ Mo-DCs (data not shown). Recognition of microbial signals by inflammasome proteins, such as NLRP3 and AIM2, triggers assembly of the inflammasome. Upon formation of the inflammasome complex, procaspase-1 is cleaved into an active cysteine protease, which further cleaves IL-1β into mature forms (35). To test the functional role of inflammasome activation for IL-1β production in CAWS-induced arteritis, groups of *Aim2*$^{-/-}$, *Nlrp3*$^{-/-}$ or *Caspase-1*$^{-/-}$ mice were

injected with CAWS and vasculitis was histologically evaluated. Deficiency of *Nlrp3, Caspase-1* and *IL-1α/β* protected mice from arteritis, whereas mice deficient in *Aim2* developed full arteritis (**Fig. 8, C and D)**.

NLRP3 inflammasome activation requires 2 signals: "signal 1" NF-κB activation inducing the transcription of NLRP3 and pro-IL-1β; and "signal 2" NLRP3 inflammasome activation inducing the cleavage of pro-IL-1β into bioactive IL-1β (36). To investigate whether CAWS directly induced IL-1β production, BMDC from *Aim2*$^{-/-}$, *NLRP3*$^{-/-}$ or *Caspase-1*$^{-/-}$ mice were stimulated with CAWS with or without the signal 1 inducer LPS or the signal 2 inducer monosodium urate crystals (MSU) for 18h, and IL-1β release was determined. In combination with either LPS or MSU, CAWS synergistically promoted IL-1β secretion in a NLRP3- and Caspase-1-dependent manner **(Fig. 8E)**. These results indicate that CAWS induces NLRP3/Caspase-1-dependent IL-1β maturation in DCs, which is required for CAWS-induced arteritis. Further, since CAWS synergized with both signal 1 and signal 2 inducers, this suggest that CAWS can act as both a signal 1 and signal 2 inducer.

BMDC from *Dectin-1*$^{-/-}$, *Dectin-2*$^{-/-}$ or *Card9*$^{-/-}$ mice were also stimulated with CAWS with or without the signal 2 stimulator MUC for 18h, and IL-1β release was determined. Secretion of IL-1β from CAWS-stimulated BMDCs was not observed in *Dectin-2*$^{-/-}$ and *Card9*$^{-/-}$ cells (**Fig. 8F**). Similar results were obtained from *Dectin-2*$^{-/-}$ Mo-DCs (data not shown). These results demonstrate that CAWS directly acts as a "signal 1" and "signal 2" via Dectin-2 activation to induce the production of IL-1β in Mo-DC, which are the major IL-1β-producers on day 7.

Role of IL-1β for chemokine and adhesion molecule expression.

MyD88 is required for most TLR signaling as well as for IL-1 receptor 1 (IL-1R1) signaling. To investigate whether MyD88 signaling in radiosensitive cells or radioresistant cells was required for CAWS-induced vasculitis, we generated BMC mice using WT and *MyD88*$^{-/-}$ mice (**Fig. 9A**). *MyD88*$^{-/-}$→ *MyD88*$^{-/-}$ controls were resistant to arteritis as were WT → *MyD88*$^{-/-}$ BMC. However, *MyD88*$^{-/-}$→ WT BMC developed arteritis comparable to WT → WT controls (**Fig. 9, B and C**). These results indicate that IL-1R1/MyD88 signaling in radioresistant cells, such as endothelial cells, is necessary for arteritis, whereas TLRs or IL-1R1/MyD88 signaling in hematopoietic cells do not contribute to the development of CAWS-induced arteritis.

To determine whether IL-1β was an important mediator of chemokine and adhesion molecule induction in the model, we stimulated mouse aortic endothelial cells (MAEC) with IL-1β and measured chemokine and adhesion molecule expression by ELISA and flow cytometry, respectively. In MAEC, IL-1β stimulated the production of chemokine proteins mediating monocyte and neutrophil recruitment, such as CCL2 and CXCL1, respectively (**Fig. 9D**). The cell surface expression of ICAM-1, VCAM-1, E-selectin and P-selectin were also elevated in IL-1β stimulated MAEC (**Fig. 9E**). Similarly, IL-1β also stimulated monocyte- and neutrophil-attracting chemokine production from primary cardiac fibroblasts **(Supplemental Fig. 8)**. We have also performed immunofluorescent staining of ICAM-1, VCAM-1 and CD31 on heart tissue isolated on day 28 after CAWS injection **(Supplemental Fig. 9)**. ICAM-1 was stained within the adventitial vessels, whereas VCAM-1 was stained in the media of the aortic root. In addition to endothelial cells, mouse

VCAM-1 is known to be expressed by hematopoietic cells, such as macrophages, granulocytes and T cells. It is presumed that in this vasculitis model, IL-1β promotes ICAM-1 expression in the adventitial vasa vasorum, driving adhesion and recruitment of inflammatory cells into the aortic root area.

To determine the role of Dectin-2 and IL-1β for chemokine induction in cardiac tissue in vivo, we measured the levels of chemokine mRNA by qPCR in *IL1a*$^{-/-}$*IL1b*$^{-/-}$ and *Dectin-2*$^{-/-}$ mice on day 28 following CAWS injection. We observed markedly reduced levels of mRNA for monocyte-attracting CCR2 chemokine ligands, such as CCL2, CCL7 and CCL12, in *IL1a*$^{-/-}$*IL1b*$^{-/-}$ and *Dectin-2*$^{-/-}$ mice compared to WT mice. In addition, levels of mRNA for the neutrophil-attracting CXCR2 chemokine ligands CXCL1, CXCL5 and CXCL7 were also decreased in *IL1a*$^{-/-}$*IL1b*$^{-/-}$ and *Dectin-2*$^{-/-}$ mice (**Fig. 9F**). Accordingly, levels of mRNA for CCR2 as well as CCR1 and CXCR2 (murine neutrophil-attracting chemokine receptors) were reduced in the hearts of *IL1a*$^{-/-}$*IL1b*$^{-/-}$ and *Dectin-2*$^{-/-}$ mice on day 28 following CAWS injection compared to WT mice (**Fig. 9G**). These data suggest that chemokines and chemokine receptors important for iMo and neutrophil recruitment are expressed in the heart in the later phase of arteritis in a Dectin-2- and IL-1α/β-dependent manner.

Discussion

CAWS is a mannoprotein-beta-glucan complex produced and secreted by *Candida albicans* that induces cardiac arteritis resembling human KD when injected intraperitoneal into mice. CAWS is non-infectious since it does not contain live fungal cells, and is considered a PAMP that activates the innate immune response (37). Here we found that CAWS directly stimulated F4/80^{+} cardiac tissue-resident macrophages (TRMs) in the adventitia of the aortic root and coronary arteries to produce CCL2 in a Dectin-2-dependent manner. CCL2 induced iMo recruitment into the adventitia of the aortic root and coronary areteries of the heart where they differentiated into Mo-DC, amplifying vessel inflammation by producing IL-1β, which resulted in neutrophil- and monocyte-attracting chemokine release from endothelial cells and fibroblasts leading to the massive inflammatory cell infiltration **(Supplemental Fig. 10)**. Strikingly, the CCR2 ligand CCL2 was exclusively expressed in the aortic root area after CAWS injection, suggesting that tissue-specific expression of CCL2 directs vascular inflammation in this model.

TRM consist of heterogeneous populations of macrophages distributed throughout the body that facilitate homeostasis and immunosurveillance (38). Tissue heterogeneity of TRM is programmed by local factors derived from tissue environments, which induce selective genetic and epigenetic programs that define the phenotype and function of TRM (39, 40). In fact, it has been demonstrated that TRM from different tissue, such as the heart, brain, lung and peritoneal cavity, have a different transcriptome, and that the CCR2 ligand CCL2 is expressed at 200-fold higher levels in cardiac macrophages compared to other TRM (41). In addition, TRM are equipped with a variety of PRR that sense microorganisms and

produce cytokines and chemokines to recruit and activate immune cells (42). Here we have found that cardiac TRM play an important role in initiating vasculitis by sensing CAWS via Dectin-2 and releasing CCL2. *Ccr2*$^{-/-}$ mice have shown to be protected against CAWS-induced vasculitis (43), which is consistent with our findings. While this prior study found that iMo were mobilized from the bone marrow in a *Ccr2*-dependent manner, they did not demonstrate that CCR2 also controls iMo entry into the heart where they contribute to vessel inflammation. Although we found that CCL2 was exclusively induced in the heart after CAWS injection in vivo, CAWS was able to induce CCL2 in vitro in TRM isolated from other organs, and Dectin-2 RNA was detected in the spleen and lung as well as the heart at baseline (data not shown). We found that CAWS components are delivered to the aortic root area of the heart on day 1 following CAWS injection, whereas they were barely detectable in other organs and in the myocardium of the heart. The preferential deposition of CAWS PAMPS may explain the mechanism of cardiac-specific induction of CCL2 in this model.

Consistent with our data, Dectin-2 has been shown to be required for CAWS-induced IL-1β production by BMDC, and that CAWS stimulation activates Syk, MAPKs and NF-κB in BMDC in a Dectin-2-dependent manner in vitro (20). We now demonstrate that Dectin-2 is required for CAWS-induced vasculitis in vivo and IL-1β production in vitro. We also found that: 1) IL-1β was markedly induced in the inflamed heart; 2) production of IL-1α/β from hematopoietic cells was required for CAWS-induced vasculitis; and 3) MyD88, which mediates IL-1R1-signaling, was required in stromal cells for CAWS-induced vasculitis. Among the myeloid cell populations, IL-1β was mainly produced by Mo-DC in

the middle phase of vasculitis (day 7), whereas neutrophils were the main IL-1β producers in the early (day 1) and late phases (day 28). In addition, we demonstrated that $CD11c^+$ cell-specific deletion of the Dectin-2-signaling molecule Syk, attenuated both IL-1β production in the heart and the induction of vasculitis. Our findings indicate that iMo recruited by CCL2-producing cardiac TRM differentiate into Mo-DC in the middle phase of vasculitis, and produce IL-1β to propel neutrophilic inflammation in the late phase. This multi-step immune cell-mobilization system might explain the relatively long period of time (−28 days) for establishing full vasculitis in this model.

GM-CSF production from radioresistant cardiac fibroblasts has also been shown to be required for CAWS-induced vasculitis (25). Since Dectin-2-expression is restricted to myeloid cells (44), it is likely that cardiac fibroblasts are not directly responding to CAWS, but instead are stimulated by cytokines, such as IL-1β, to produce GM-CSF. As IL-1β is known to be a classical inducer of GM-CSF in physiological and pathological conditions (45), and IL-1β promotes GM-CSF production from fibroblasts (46), IL-1β is a potential upstream stimulator of fibroblast-derived GM-CSF production. However, Stock et al. have argued that IL-1 signaling is not essential for the development of cardiac vasculitis. Their conclusion was based on their findings that *IL-1r1*-deficient mice had no impairment in neutrophil and monocyte infiltrate into the heart 1 day after CAWS injection, and that Anakinra, an IL-1 receptor antagonist (IL-1Ra), did not attenuate CAWS-induced vasculitis. In contrast, we have found that *IL1a*$^{-/-}$*IL1b*$^{-/-}$ mice were completely protected from vasculitis by histological analysis on day 28. A possible explanation for this discrepancy is that Stock et al. did not analyze the hearts of *IL-1r1*$^{-/-}$ mice histopathologically on day 28. It is likely

that IL-1 is not involved in the initial inflammatory cell recruitment on day 1, but instead required for the establishment of vasculitis in the late phase. Further, Anakinra has a short half-life (4-6h) (47), and therefore is usually administered once or twice daily for the treatment of inflammatory diseases in humans and mice. Evidence from preclinical models of disease indicate that the therapeutic effectiveness of Anakinra is crucially dependent on the continuous saturation of IL-1 receptors (48). Therefore the 3 times a week dosing of Anakinra by Stock et al. may not have been sufficient to neutralize all of IL-1 activity in the model. Supporting a role for IL-1 in KD-like vasculitis, IL-1β has been shown to be required for the LCWE-induced mouse model of KD (49), and *IL-1ra*$^{-/-}$ mice spontaneously develop aortitis (50).

Growing experimental evidence supports a paradigm of "outside-in" inflammation in vasculitis, in which vascular inflammation is initiated and perpetuated in the adventitia and progress inward to the intima (51). In CAWS-induced vasculitis, it has been demonstrated that vascular inflammation starts from the neovascularization of the vasa vasorum in adventitia of the aorta followed by inflammatory cell accumulation (52). This is consistent with our observation that following deposition CAWS in the aortic root TRM residing in the adventitia initiate vascular inflammation. Clinically, KD is classified as a medium-vessel vasculitis as small vessels are not commonly affected (53). In contrast, antineutronphil cytoplasmic antibody-associated vasculitis (AAV) is classified as a small vessel vasculitis as small vessels, and not medium sized vessels, are commonly involved in this disease. Interestingly, the concept of pathogen-triggered activation of immune cells is accepted as one of the major triggers of AAV (54). Our finding that the location of antigen deposition

determines the site of vascular inflammation in the CAWS model could provide a clue to solve the long-standing question of why specific vasculitis syndromes occur in specific vessels and not in all vessels and in all organs throughout the body.

Some limitations in the present study need to be considered. First, although the CAWS-induced vasculitis model is considered as a representative animal model of KD (11, 12, 55), like all other animal disease models, it is not identical to the human disease, especially since the trigger for the development of KD is not known. However, the distribution of arterial lesions and the histological features of the vascular lesions in this model are similar to those in KD, which are both characterized by necrotizing vasculitis with granulomatous inflammation (11). The CAWS-induced model is suitable for studying the mechanisms by which PAMPs can induce vascular inflammation, which may be of relevance to human vasculitis but caution is needed when applying the results from mouse models directly to human disease. Second, we focused mainly on the role of myeloid cell subsets, but did not evaluate other immune cells, such as T cells, B cells and NK cells. Taking into account the time lag between CAWS administration and established vasculitis, it is presumed that in addition to the innate immune response initiated by Dectin-2, there is also activation of the adaptive immune response that likely contributes to cardiac inflammation. Third, we have tested $CD11c^+$ cell-specific Syk deletion in order to assess the contribution of Dectin-2 signaling in $CD11c^+$ cells, as Dectin-2-floxed mice are not available. However, another CLR, Mincle also interacts with FcRγ to activate Syk (56). As Mincle also recognizes mannose-rich *Candida* structures, Syk-deletion could also influence Mincle-mediated signaling in vivo. Fourth, we do not understand why intraperitoneally-injected CAWS is

preferentially transported and or captured in the aortic root area of the heart and further study will be required to delineate the mechanism.

Increasing numbers of studies have implicated infection as risk factors for KD (8). Our findings demonstrate that Candidal PAMPs initiate arteritis by activating TRM in the aortic root and inducing chemokine and cytokine production in a mouse model of vasculitis resembling KD. Several case reports have shown promising results using the IL-1 receptor antagonist Anakinra to treat KD (57, 58) and new therapeutics that target the CCL2/CCR2 chemokine axis are currently in clinical trials for cancer (59, 60). Finally, Syk inhibitors are available and have been in clinical trials for the treatment of rheumatoid arthritis (61). Thus, the critical pathways that we have identified that mediate CAWS-induced vasculitis can be tested as potential new therapeutic targets for combating KD.

Methods

Mice.

LysM-GFP (28), *Ccr2*$^{RFP/RFP}$ (29), *Dectin-1* $^{-/-}$ (62), *Dectin-2* $^{-/-}$ (20), *IL1a*$^{-/-}$*IL1b*$^{-/-}$ (63), *Card9*$^{-/-}$ (64), and *pIL1-DsRed* (34) mice were maintained in our laboratory. Wild-type C57BL/6 and congenic CD45.1 mice were purchased from Charles River Laboratories. *Tlr2*$^{-/-}$, *Tlr4*$^{-/-}$, *Aim2*$^{-/-}$, *Nlrp3*$^{-/-}$, *Caspase-1*$^{-/-}$, *FcγR*$^{-/-}$, *MyD88*$^{-/-}$, *Ccl2-RFP*^{flox}, Syk$^{fl/fl}$ and CD11c-Cre mice were purchased from Jackson laboratory. CD11cCre-Syk$^{fl/fl}$ mice were generated by crossing Syk$^{fl/fl}$ mice with CD11c-Cre mice. All the mice were in the C57BL/6 genetic background.

Induction of CAWS-induced arteritis.

CAWS was prepared from *C. albicans* strain IFO1385, using a previously described method (65). To induce vasculitis, CAWS (1 mg) was injected intraperitoneally into the mice once daily for 5d. Hearts were perfused with PBS and fixed with 10% formalin. Multiple paraffin-embedded 5-mm sections were prepared and stained with hematoxylin and eosin (H&E). To quantitatively evaluate vascular inflammation, each of 5 areas (3 aortic root areas and both coronary arteries) was scored 0–3 according to the classification system for the areas of cellular infiltration: (a) aortic root (score 0 for no inflammation; 1, cell infiltration <100 um in diameter; 2, 100–199 um in diameter; 3, ≥200 um in diameter); (b) coronary arteries (score 0 for no inflammation; 1, cell infiltration <50 um in diameter; 2, 50–99 um in diameter; 3, ≥100 um in diameter). The severity of arteritis in each mouse was defined as the sum of the scores of the five segments (maximum possible score of 15).

Parabiosis.

CD45.2$^+$ C57BL/6 mice and naive CD45.1$^+$ C57BL/6 mice underwent hair removal along opposite lateral flanks with the use of hair clippers and depilatory cream. Skin was then wiped clean of fur with 70% alcohol prep pads and betadine solution. Mirrored incisions were then made on the lateral aspects of both mice. 4.0 sutures were placed around the olecranon joints as well as the knees joints of both mice to secure the upper and lower extremities, respectively. Dorsal and ventral skin was approximated with the use of 4.0 sutures and surgical staples to conjoin the mice. At the end of the surgery, mice received subcutaneous enrofloxacin antibiotic as well as buprenorphine and flunixin for pain control. Enrofloxacin antibiotic was subsequently administered via drinking water. Subcutaneous buprenorphine and flunixin was administered as needed every 12h for 48h. Recirculation was assessed in peripheral blood 4wk after surgery.

In vivo adoptive cell transfer.

Bone marrow derived monocytes (BMDM) were negatively isolated using a mouse monocyte isolation kit (Stem Cell Technologies) from *LysM*-GFP or *Ccr2*$^{RFP/RFP}$ mice. The cells were counted and resuspended in PBS containing 1% FCS at 0.5x 10^5 cells/100 µl. For competitive adoptive transfer experiments, the cells were intravenously injected at a 1:1 ratio into WT recipient mice (200 ul/mouse) along with intraperitoneal CAWS (1 mg) injection **(Fig. 2C)**. 20h after cell transfer, peripheral blood and hearts of recipient mice were analyzed. Proportion of donor-derived GFP$^+$ and RFP$^+$ cells in the heart was detected by flow cytometry. For tracking the transferred BMDM, *LysM*-GFP mouse BMDM were intravenously injected 0.5× 10^5 per mouse, once daily for 5d along with i.p. injection of

CAWS (1 mg) **(Fig. 2F)**. GFP^+ cell population before adoptive transfer and those recovered from heart 7d after initial CAWS injection were analyzed by flow cytometry.

Immunohistochemistry.

Paraffin-embedded mouse hearts were deparaffinized and then immersed in citrate buffer (F4/80) or Borg decloaker (Ly6G/Ly6C) for 45min at 95-97˚C, removed from heat, and kept at room temperature for 20min. Endogenous peroxidase activity was blocked by incubation in endogenous peroxidase and alkaline phosphatase blocking solution (Vector laboratories) for 10min. Sections were then blocked with 5% normal goat serum for 60min and stained with rabbit anti-F4/80 polyclonal antibody (Cell Signaling) or rat anti-Ly6G/Ly6C mAb (Novus Bio) overnight at 4˚C. Antibody binding was amplified using SignalStain boost IHC detection reagent (Cell Signaling) or ImmPRESS polymer reagents (Vector laboratories) and developed with DAB. The slides were examined using a bright field microscope (Carl Zeiss).

Immunofluorescence microscopy.

OCT-embedded tissue sections (7 μm thick) from frozen heart tissue were prepared as described. Sections were then blocked with protein block (DakoCytomation) for 15min and stained with rat anti-CD11b biotinylated antibody (Biolegend), Armenian hamster anti-CD11c biotinylated antibody (Biolegend), rat anti-Ly6G biotinylated antibody (Biolegend), or rat anti-Dectin-2 antibody (Bio-Rad) for 60min at 25°C. Streptavidin-FITC (BD Biosciences) or Alexa Fluor 488–conjugated goat anti-rat IgG antibody (Invitrogen) was

used as a secondary antibody and incubated for 30min at 25°C. The slides were examined using a fluorescence microscope (Carl Zeiss).

Generation of BMC mice.

BMC mice were generated according to established protocols (66). Eight weeks after reconstitution BMC mice were used for experiments. The recovery of blood cell counts at 8 weeks after irradiation was confirmed by WBC differential count. FACS analysis of CD45.1 and CD45.2 expression on BM-derived blood cells was used to control for chimerism, exploiting the congenic expression of the CD45.1 allele in WT mice vs. CD45.2 expression in *IL1a*$^{-/-}$*IL1b*$^{-/-}$ or *MyD88*$^{-/-}$ mice. Staining reagents used were anti-CD45.1-FITC and anti-CD45.2-APC (BioLegend). BMC mice were used if ≥ 95% of leukocytes were of donor origin.

BMDC preparation.

Femurs were removed from the mice and the BM was flushed out and plated in petri dishes with media containing GM-CSF (20 ng/mL; PeproTech). After 7d in culture, BMDCs (1×10^6cells/mL) were plated in six- or 96-well plates and then stimulated with CAWS (100 ug/ml), LPS (1 ug/ml; Sigma-Aldrich), or monosodium urate crystals (MUC) (100 ug/ml; Invivogen) for 18h. Cell supernatants were analyzed for IL-1β by ELISA (R&D Systems). Cell lysates and concentrated culture *supernatants* were used for immunoblot analysis.

Flow cytometry.

The hearts were minced and digested with 450 U/ml collagenase I, 125 U/ ml collagenase XI, 60 U/ml DNase I, and 60 U/ml hyaluronidase (Sigma-Aldrich) in PBS for 1h at 37°C with shaking (67). A cell suspension was obtained by mashing the tissue through a 70-um strainer. Single cells were incubated with anti-mouse CD16/32 (93, TruStain fcX, BioLegend) to block Fc receptors and then stained with Fixable Viability Dye eF780 (eBioscience) to identify dead cells and fluorochrome-conjugated anti-mouse Abs as indicated in Supplemental Table 1. In preliminary experiments, i.v. CD45 mAb was administered 3min before harvesting to distinguish intravascular leukocytes that remain even after vigorous flushing from truly intraparenchymal leukocytes. As has been described (68), in contrast to other organs like the lung, we only found that ~10% of the leukocytes stained with i.v. CD45 (data not shown). Therefore, we did not routinely perform this technique for this study that exclusively focused on the heart.

Quantitive real-time PCR.

Tissue was isolated and homogenized in Trizol (Sigma-Aldrich) and RNA was isolated according to the manufacture's instruction. Purified RNA was then converted to cDNA by reverse transcription (TaqMan Reverse Transcriptase Reagents, Themofisher). qPCR reactions in the presence of SYBR Green (FastStart Essential DNA Green Master Mix, Roche) were performed on a LightCylcer 96 Instrument (Roche) and normalized to *β2m*. The sequences for the qPCR primers can be found in Supplemental Table 2.

Quantitative immunofluorescence analysis of NF-κB nuclear translocation.

BMDCs were plated and cultured on recombinant ICAM-1 (2.5 ug/ml; Biolegend)-coated glass coverslips at a density of $2x10^5$ cells per well in 8-well plates. The cells were treated with CAWS (100ug/ml), LPS (1 ug/ml; Sigma-Aldrich) or PBS for 60min at 37˚C. Then the cells were fixed with 4% formalin in PBS for 15min at room temperature. They were then permeabilized with PBS containing 1% Triton X-100 for 10min at room temperature. To block the nonspecific binding of the antibodies, samples were incubated with protein block (DakoCytomation) for 15min at room temperature. Rabbit mAb for NF-κB p65 (1:400; Cell Signaling Technology) was added to the samples and incubated 18h at 4˚C. Then the cells were incubated with anti-rabbit secondary antibody conjugated with Alexa 546 (Invitrogen) for 30min at room temperature. Nuclear:cytoplasmic ratios of NF-κB p65 was analyzed using a fluorescence microscope (Carl Zeiss).

In vitro cardiac macrophage stimulation.

Single cell suspension derived from heart was passed through 30 um cell strainer twice followed by incubation with anti-F4/80 microbeads (Miltenyi Biotec). Beads conjugated $F4/80^+$ cells were magnetically isolated by magnetic-activated cell sorting (MACS). $F4/80^+$ cells were plated at a density of $1x10^5$ cells per well in 96-well plates. The cells were treated with CAWS (10 ug/ml) or PBS for 18h at 37˚C. Cell-free cell culture supernatants were assayed for CCL2 (R&D Systems) by ELISA.

In vitro mouse aortic endothelial cell stimulation.

C57BL/6 mouse primary aortic endothelial cells were purchased from CellBiologics. The cells were seeded at 1×10^5 in 24 well plates and cultured in endothelial cell medium

(CellBiologics) at 37°C. Cultures were stimulated with recombinant IL-1β (20 ng/ml; Biolegend) for 18h. Then the cells were stained for flow cytometry and the chemokine levels in the culture supernatants were assessed by Multi-Analyte ELISArray Kit (Qiagen).

In vitro mouse cardiac fibroblasts stimulation.

C57BL/6 mouse primary cardiac fibroblasts were purchased from CellBiologics. The cells were seeded at 2 x 10^4 in 96 well plates and cultured in complete DMEM at 37°C. Cultures were stimulated with CAWS (10 ug/ml, 100 ug/ml or 1 mg/ml), recombinant IL-1β (50 ng/ml; Biolegend), recombinant TNFα (50 ng/ml; PeproTech) or LPS (50 mg/ml; Sigma-Aldrich) for 18h. Cell lysates were used for qPCR analysis. Cell-free cell culture supernatants were assayed for CCL2 (R&D Systems) by ELISA.

Statistical analysis. Data were analyzed using Prism7 (GraphPad Software Inc.), and results were expressed as the mean ±SEM. P value in multiple groups was calculated using ordinary one-way ANOVA with Dunnett's post-hoc test or Tukey's multicomparison test as appropriate. Means between two groups were compared with unpaired two-tailed Student's t test. A P value less than 0.05 was considered significant.

Study approval. All experiments described herein were approved by the IACUC of Massachusetts General Hospital.

Author Contributions

C.M. designed and performed most experiments, analyzed and interpreted data and contributed to writing the manuscript; Y.M. performed and analyzed BMC and in vivo adoptive transfer experiments; L.M. assisted in the qPCR, ELISA and IHC experiments; J.L. provided technical assistance for the flow cytometry and qPCR experiments; R.A.R. generated parabiotic mice; N.N.M. and N.O. provided CAWS; Y.I. provided *IL1a*$^{-/-}$*IL1b*$^{-/-}$ mice, *Dectin-1*$^{-/-}$ mice and *Dectin-2*$^{-/-}$ mice; T.K. supervised the project; A.D.L. provided overall project supervision, contributed to the design of the experiments and wrote the manuscript.

Acknowledgements

This work is funded by National Institutes of Health grant R01AI050892 and Rheumatology Research Foundation to ADL, and Japan Heart Association and Japan Blood Products organization to CM. The authors thank N. Barrett (Brigham and Women's Hospital, Boston) for *Dectin-1* and *Dectin-2*-deficient mice, R. Xavier (Massachusetts General Hospital, Boston) for *Card9*-deficient mice and S. Lacroix (Laval University, Québec City) for *Ccl2-RFP*$^{fl/fl}$ reporter mice. We would also like to thank A. Sato and S. Ji for their technical support.

References

1. Kawasaki T. [Acute febrile mucocutaneous syndrome with lymphoid involvement with specific desquamation of the fingers and toes in children]. *Arerugi.* 1967;16(3):178-222.
2. Taubert KA, Rowley AH, and Shulman ST. Seven-year national survey of Kawasaki disease and acute rheumatic fever. *Pediatr Infect Dis J.* 1994;13(8):704-8.
3. Takahashi K, Oharaseki T, Yokouchi Y, Hiruta N, and Naoe S. Kawasaki disease as a systemic vasculitis in childhood. *Ann Vasc Dis.* 2010;3(3):173-81.
4. Kato H, Sugimura T, Akagi T, Sato N, Hashino K, Maeno Y, Kazue T, Eto G, and Yamakawa R. Long-term consequences of Kawasaki disease. A 10- to 21-year follow-up study of 594 patients. *Circulation.* 1996;94(6):1379-85.
5. Newburger JW, Takahashi M, Beiser AS, Burns JC, Bastian J, Chung KJ, Colan SD, Duffy CE, Fulton DR, Glode MP, et al. A single intravenous infusion of gamma globulin as compared with four infusions in the treatment of acute Kawasaki syndrome. *N Engl J Med.* 1991;324(23):1633-9.
6. Greco A, De Virgilio A, Rizzo MI, Tombolini M, Gallo A, Fusconi M, Ruoppolo G, Pagliuca G, Martellucci S, and de Vincentiis M. Kawasaki disease: An evolving paradigm. *Autoimmun Rev.* 2015;14(8):703-9.
7. Burns JC, and Glode MP. Kawasaki syndrome. *Lancet.* 2004;364(9433):533-44.
8. Wang CL, Wu YT, Liu CA, Kuo HC, and Yang KD. Kawasaki disease: infection, immunity and genetics. *Pediatr Infect Dis J.* 2005;24(11):998-1004.
9. Xie X, Shi X, and Liu M. The Roles of Genetic Factors in Kawasaki Disease: A Systematic Review and Meta-analysis of Genetic Association Studies. *Pediatric cardiology.* 2018;39(2):207-25.
10. Luzina IG, and Handwerger BS. Lessons from animal models of vasculitis. *Current rheumatology reports.* 2000;2(5):369-75.
11. Takahashi K, Oharaseki T, Wakayama M, Yokouchi Y, Naoe S, and Murata H. Histopathological features of murine systemic vasculitis caused by Candida albicans extract--an animal model of Kawasaki disease. *Inflamm Res.* 2004;53(2):72-7.
12. Miyabe C, Miyabe Y, Miura NN, Takahashi K, Terashima Y, Toda E, Honda F, Morio T, Yamagata N, Ohno N, et al. Am80, a retinoic acid receptor agonist, ameliorates murine vasculitis through the suppression of neutrophil migration and activation. *Arthritis and rheumatism.* 2013;65(2):503-12.
13. Lehman TJ, Walker SM, Mahnovski V, and McCurdy D. Coronary arteritis in mice following the systemic injection of group B Lactobacillus casei cell walls in aqueous suspension. *Arthritis and rheumatism.* 1985;28(6):652-9.
14. Nishio H, Kanno S, Onoyama S, Ikeda K, Tanaka T, Kusuhara K, Fujimoto Y, Fukase K, Sueishi K, and Hara T. Nod1 ligands induce site-specific vascular inflammation. *Arteriosclerosis, thrombosis, and vascular biology.* 2011;31(5):1093-9.
15. Rodo X, Ballester J, Cayan D, Melish ME, Nakamura Y, Uehara R, and Burns JC. Association of Kawasaki disease with tropospheric wind patterns. *Scientific reports.* 2011;1(152.
16. Rodo X, Curcoll R, Robinson M, Ballester J, Burns JC, Cayan DR, Lipkin WI, Williams BL, Couto-Rodriguez M, Nakamura Y, et al. Tropospheric winds from

northeastern China carry the etiologic agent of Kawasaki disease from its source to Japan. *Proceedings of the National Academy of Sciences of the United States of America.* 2014;111(22):7952-7.
17. El-Askary H, LaHaye N, Linstead E, Sprigg WA, and Yacoub M. Remote sensing observation of annual dust cycles and possible causality of Kawasaki disease outbreaks in Japan. *Global cardiology science & practice.* 2017;2017(3):e201722.
18. Ishibashi K, Fukazawa R, Miura NN, Adachi Y, Ogawa S, and Ohno N. Diagnostic potential of antibody titres against Candida cell wall beta-glucan in Kawasaki disease. *Clin Exp Immunol.* 2014;177(1):161-7.
19. Takeuchi O, and Akira S. Pattern recognition receptors and inflammation. *Cell.* 2010;140(6):805-20.
20. Saijo S, Ikeda S, Yamabe K, Kakuta S, Ishigame H, Akitsu A, Fujikado N, Kusaka T, Kubo S, Chung SH, et al. Dectin-2 recognition of alpha-mannans and induction of Th17 cell differentiation is essential for host defense against Candida albicans. *Immunity.* 2010;32(5):681-91.
21. Brown GD. Dectin-1: a signalling non-TLR pattern-recognition receptor. *Nat Rev Immunol.* 2006;6(1):33-43.
22. McGreal EP, Rosas M, Brown GD, Zamze S, Wong SY, Gordon S, Martinez-Pomares L, and Taylor PR. The carbohydrate-recognition domain of Dectin-2 is a C-type lectin with specificity for high mannose. *Glycobiology.* 2006;16(5):422-30.
23. Drummond RA, Saijo S, Iwakura Y, and Brown GD. The role of Syk/CARD9 coupled C-type lectins in antifungal immunity. *European journal of immunology.* 2011;41(2):276-81.
24. Netea MG, Gow NA, Munro CA, Bates S, Collins C, Ferwerda G, Hobson RP, Bertram G, Hughes HB, Jansen T, et al. Immune sensing of Candida albicans requires cooperative recognition of mannans and glucans by lectin and Toll-like receptors. *The Journal of clinical investigation.* 2006;116(6):1642-50.
25. Stock AT, Hansen JA, Sleeman MA, McKenzie BS, and Wicks IP. GM-CSF primes cardiac inflammation in a mouse model of Kawasaki disease. *J Exp Med.* 2016.
26. Tamoutounour S, Guilliams M, Montanana Sanchis F, Liu H, Terhorst D, Malosse C, Pollet E, Ardouin L, Luche H, Sanchez C, et al. Origins and functional specialization of macrophages and of conventional and monocyte-derived dendritic cells in mouse skin. *Immunity.* 2013;39(5):925-38.
27. Dominguez-Andres J, Feo-Lucas L, Minguito de la Escalera M, Gonzalez L, Lopez-Bravo M, and Ardavin C. Inflammatory Ly6Chigh Monocytes Protect against Candidiasis through IL-15-Driven NK Cell/Neutrophil Activation. *Immunity.* 2017;46(6):1059-72 e4.
28. Faust N, Varas F, Kelly LM, Heck S, and Graf T. Insertion of enhanced green fluorescent protein into the lysozyme gene creates mice with green fluorescent granulocytes and macrophages. *Blood.* 2000;96(2):719-26.
29. Saederup N, Cardona AE, Croft K, Mizutani M, Cotleur AC, Tsou CL, Ransohoff RM, and Charo IF. Selective chemokine receptor usage by central nervous system myeloid cells in CCR2-red fluorescent protein knock-in mice. *PLoS One.* 2010;5(10):e13693.
30. Shi C, Jia T, Mendez-Ferrer S, Hohl TM, Serbina NV, Lipuma L, Leiner I, Li MO, Frenette PS, and Pamer EG. Bone marrow mesenchymal stem and progenitor cells

induce monocyte emigration in response to circulating toll-like receptor ligands. *Immunity.* 2011;34(4):590-601.
31. Netea MG, Van Der Graaf CA, Vonk AG, Verschueren I, Van Der Meer JW, and Kullberg BJ. The role of toll-like receptor (TLR) 2 and TLR4 in the host defense against disseminated candidiasis. *The Journal of infectious diseases.* 2002;185(10):1483-9.
32. Saijo K, Schmedt C, Su IH, Karasuyama H, Lowell CA, Reth M, Adachi T, Patke A, Santana A, and Tarakhovsky A. Essential role of Src-family protein tyrosine kinases in NF-kappaB activation during B cell development. *Nat Immunol.* 2003;4(3):274-9.
33. Caton ML, Smith-Raska MR, and Reizis B. Notch-RBP-J signaling controls the homeostasis of CD8- dendritic cells in the spleen. *J Exp Med.* 2007;204(7):1653-64.
34. Matsushima H, Ogawa Y, Miyazaki T, Tanaka H, Nishibu A, and Takashima A. Intravital imaging of IL-1beta production in skin. *J Invest Dermatol.* 2010;130(6):1571-80.
35. Strowig T, Henao-Mejia J, Elinav E, and Flavell R. Inflammasomes in health and disease. *Nature.* 2012;481(7381):278-86.
36. Jo EK, Kim JK, Shin DM, and Sasakawa C. Molecular mechanisms regulating NLRP3 inflammasome activation. *Cellular & molecular immunology.* 2016;13(2):148-59.
37. Shinohara H, Nagi-Miura N, Ishibashi K, Adachi Y, Ishida-Okawara A, Oharaseki T, Takahashi K, Naoe S, Suzuki K, and Ohno N. Beta-mannosyl linkages negatively regulate anaphylaxis and vasculitis in mice, induced by CAWS, fungal PAMPS composed of mannoprotein-beta-glucan complex secreted by Candida albicans. *Biol Pharm Bull.* 2006;29(9):1854-61.
38. Davies LC, Jenkins SJ, Allen JE, and Taylor PR. Tissue-resident macrophages. *Nat Immunol.* 2013;14(10):986-95.
39. Gosselin D, Link VM, Romanoski CE, Fonseca GJ, Eichenfield DZ, Spann NJ, Stender JD, Chun HB, Garner H, Geissmann F, et al. Environment drives selection and function of enhancers controlling tissue-specific macrophage identities. *Cell.* 2014;159(6):1327-40.
40. Lavin Y, Winter D, Blecher-Gonen R, David E, Keren-Shaul H, Merad M, Jung S, and Amit I. Tissue-resident macrophage enhancer landscapes are shaped by the local microenvironment. *Cell.* 2014;159(6):1312-26.
41. Epelman S, Lavine KJ, Beaudin AE, Sojka DK, Carrero JA, Calderon B, Brija T, Gautier EL, Ivanov S, Satpathy AT, et al. Embryonic and adult-derived resident cardiac macrophages are maintained through distinct mechanisms at steady state and during inflammation. *Immunity.* 2014;40(1):91-104.
42. Taylor PR, Martinez-Pomares L, Stacey M, Lin HH, Brown GD, and Gordon S. Macrophage receptors and immune recognition. *Annu Rev Immunol.* 2005;23(901-44.
43. Martinez HG, Quinones MP, Jimenez F, Estrada C, Clark KM, Suzuki K, Miura N, Ohno N, Ahuja SK, and Ahuja SS. Important role of CCR2 in a murine model of coronary vasculitis. *BMC Immunol.* 2012;13(56.
44. Taylor PR, Reid DM, Heinsbroek SE, Brown GD, Gordon S, and Wong SY. Dectin-2 is predominantly myeloid restricted and exhibits unique activation-dependent

expression on maturing inflammatory monocytes elicited in vivo. *European journal of immunology.* 2005;35(7):2163-74.
45. Seelentag WK, Mermod JJ, Montesano R, and Vassalli P. Additive effects of interleukin 1 and tumour necrosis factor-alpha on the accumulation of the three granulocyte and macrophage colony-stimulating factor mRNAs in human endothelial cells. *Embo j.* 1987;6(8):2261-5.
46. Darrieutort-Laffite C, Boutet MA, Chatelais M, Brion R, Blanchard F, Heymann D, and Le Goff B. IL-1beta and TNFalpha promote monocyte viability through the induction of GM-CSF expression by rheumatoid arthritis synovial fibroblasts. *Mediators of inflammation.* 2014;2014(241840.
47. Braddock M, and Quinn A. Targeting IL-1 in inflammatory disease: new opportunities for therapeutic intervention. *Nature reviews Drug discovery.* 2004;3(4):330-9.
48. Bendele A, McAbee T, Sennello G, Frazier J, Chlipala E, and McCabe D. Efficacy of sustained blood levels of interleukin-1 receptor antagonist in animal models of arthritis: comparison of efficacy in animal models with human clinical data. *Arthritis and rheumatism.* 1999;42(3):498-506.
49. Wakita D, Kurashima Y, Crother TR, Noval Rivas M, Lee Y, Chen S, Fury W, Bai Y, Wagner S, Li D, et al. Role of Interleukin-1 Signaling in a Mouse Model of Kawasaki Disease-Associated Abdominal Aortic Aneurysm. *Arteriosclerosis, thrombosis, and vascular biology.* 2016;36(5):886-97.
50. Matsuki T, Isoda K, Horai R, Nakajima A, Aizawa Y, Suzuki K, Ohsuzu F, and Iwakura Y. Involvement of tumor necrosis factor-alpha in the development of T cell-dependent aortitis in interleukin-1 receptor antagonist-deficient mice. *Circulation.* 2005;112(9):1323-31.
51. Stenmark KR, Yeager ME, El Kasmi KC, Nozik-Grayck E, Gerasimovskaya EV, Li M, Riddle SR, and Frid MG. The adventitia: essential regulator of vascular wall structure and function. *Annual review of physiology.* 2013;75(23-47.
52. Hamaoka-Okamoto A, Suzuki C, Yahata T, Ikeda K, Nagi-Miura N, Ohno N, Arai Y, Tanaka H, Takamatsu T, and Hamaoka K. The involvement of the vasa vasorum in the development of vasculitis in animal model of Kawasaki disease. *Pediatr Rheumatol Online J.* 2014;12(12.
53. Jennette JC, Falk RJ, Bacon PA, Basu N, Cid MC, Ferrario F, Flores-Suarez LF, Gross WL, Guillevin L, Hagen EC, et al. 2012 revised International Chapel Hill Consensus Conference Nomenclature of Vasculitides. *Arthritis and rheumatism.* 2013;65(1):1-11.
54. Nakazawa D, Masuda S, Tomaru U, and Ishizu A. Pathogenesis and therapeutic interventions for ANCA-associated vasculitis. *Nat Rev Rheumatol.* 2019;15(2):91-101.
55. Miyabe C, Miyabe Y, Komiya T, Shioya H, Miura NN, Takahashi K, Ohno N, Tsuboi R, Luster AD, Kawai S, et al. A sphingosine 1-phosphate receptor agonist ameliorates animal model of vasculitis. *Inflamm Res.* 2016.
56. Yamasaki S, Ishikawa E, Sakuma M, Hara H, Ogata K, and Saito T. Mincle is an ITAM-coupled activating receptor that senses damaged cells. *Nat Immunol.* 2008;9(10):1179-88.

57. Guillaume MP, Reumaux H, and Dubos F. Usefulness and safety of anakinra in refractory Kawasaki disease complicated by coronary artery aneurysm. *Cardiology in the young.* 2018:1-4.
58. Kone-Paut I, Cimaz R, Herberg J, Bates O, Carbasse A, Saulnier JP, Maggio MC, Anton J, and Piram M. The use of interleukin 1 receptor antagonist (anakinra) in Kawasaki disease: A retrospective cases series. *Autoimmun Rev.* 2018.
59. Noel M, Lowery M, Ryan D, Wolpin B, Bullock A, Britten C, Jin B, Ganguly BJ, Taylor CT, Yin D, et al. 750PPhase Ib study of PF-04136309 (an oral CCR2 inhibitor) in combination with nab-paclitaxel/gemcitabine in first-line treatment of metastatic pancreatic adenocarcinoma. *Annals of Oncology.* 2017;28(suppl_5):mdx369.132-mdx369.132.
60. Noel MS, Hezel AF, Linehan D, Wang-Gillam A, Eskens F, Sleijfer S, Desar I, Erdkamp F, Wilmink J, Diehl J, et al. Orally administered CCR2 selective inhibitor CCX872-b clinical trial in pancreatic cancer. *Journal of Clinical Oncology.* 2017;35(4_suppl):276-.
61. Kunwar S, Devkota AR, and Ghimire DK. Fostamatinib, an oral spleen tyrosine kinase inhibitor, in the treatment of rheumatoid arthritis: a meta-analysis of randomized controlled trials. *Rheumatology international.* 2016;36(8):1077-87.
62. Saijo S, Fujikado N, Furuta T, Chung SH, Kotaki H, Seki K, Sudo K, Akira S, Adachi Y, Ohno N, et al. Dectin-1 is required for host defense against Pneumocystis carinii but not against Candida albicans. *Nat Immunol.* 2007;8(1):39-46.
63. Horai R, Asano M, Sudo K, Kanuka H, Suzuki M, Nishihara M, Takahashi M, and Iwakura Y. Production of mice deficient in genes for interleukin (IL)-1alpha, IL-1beta, IL-1alpha/beta, and IL-1 receptor antagonist shows that IL-1beta is crucial in turpentine-induced fever development and glucocorticoid secretion. *J Exp Med.* 1998;187(9):1463-75.
64. Hara H, Ishihara C, Takeuchi A, Imanishi T, Xue L, Morris SW, Inui M, Takai T, Shibuya A, Saijo S, et al. The adaptor protein CARD9 is essential for the activation of myeloid cells through ITAM-associated and Toll-like receptors. *Nat Immunol.* 2007;8(6):619-29.
65. Uchiyama M, Ohno N, Miura NN, Adachi Y, Aizawa MW, Tamura H, Tanaka S, and Yadomae T. Chemical and immunochemical characterization of limulus factor G-activating substance of Candida spp. *FEMS immunology and medical microbiology.* 1999;24(4):411-20.
66. Sadik CD, Kim ND, Iwakura Y, and Luster AD. Neutrophils orchestrate their own recruitment in murine arthritis through C5aR and FcgammaR signaling. *Proceedings of the National Academy of Sciences of the United States of America.* 2012;109(46):E3177-85.
67. Anzai A, Choi JL, He S, Fenn AM, Nairz M, Rattik S, McAlpine CS, Mindur JE, Chan CT, Iwamoto Y, et al. The infarcted myocardium solicits GM-CSF for the detrimental oversupply of inflammatory leukocytes. *J Exp Med.* 2017;214(11):3293-310.
68. Ramos GC, van den Berg A, Nunes-Silva V, Weirather J, Peters L, Burkard M, Friedrich M, Pinnecker J, Abesser M, Heinze KG, et al. Myocardial aging as a T-cell-mediated phenomenon. *Proceedings of the National Academy of Sciences of the United States of America.* 2017;114(12):E2420-e9.

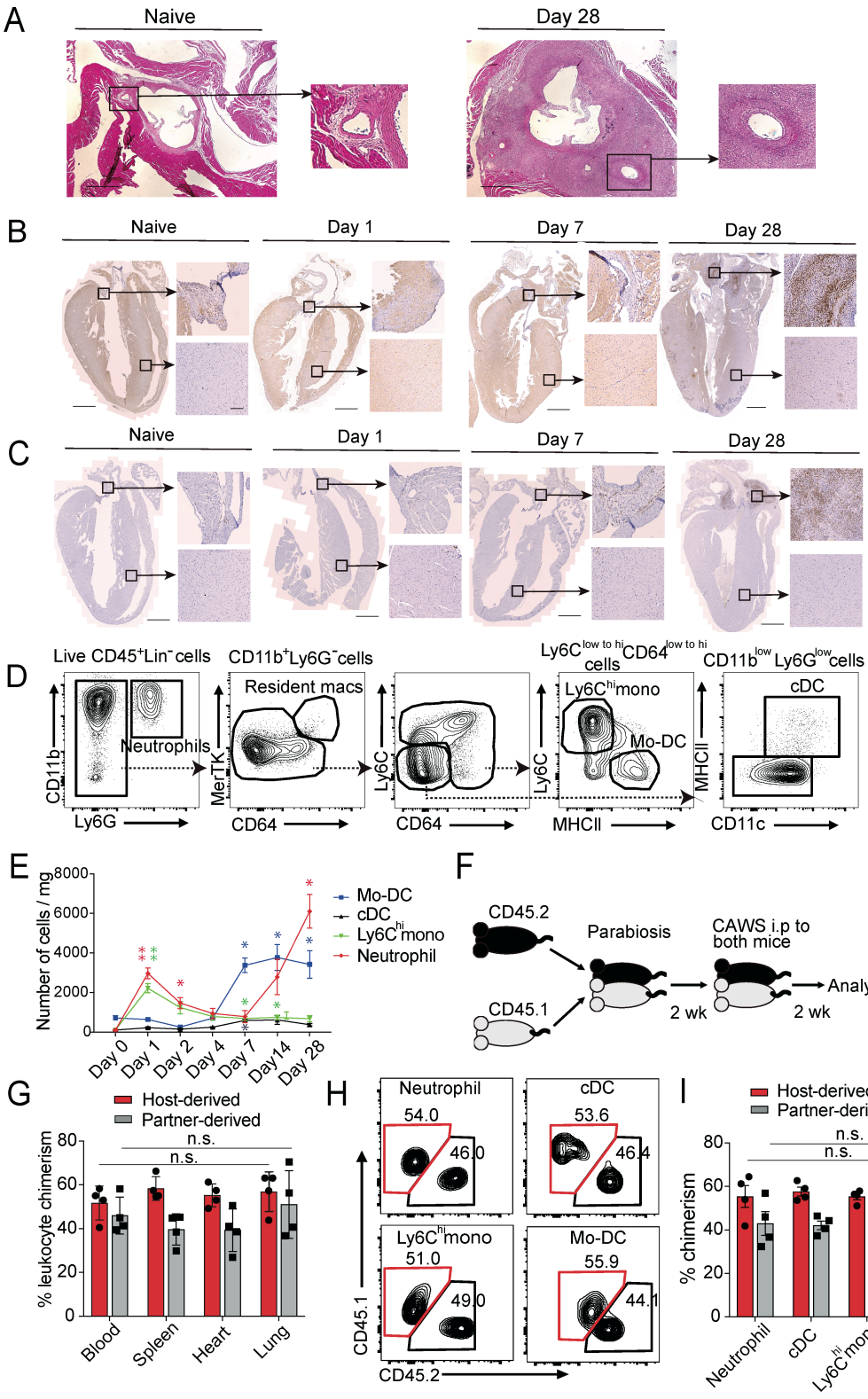
A
Naive
Day 28
B
Naive
Day 1
Day 7
Day 28
C
Naive
Day 1
Day 7
Day 28
D
Live CD45+Lin- cells
CD11b+Ly6G- cells
Ly6Clow to hi cells CD64low to hi
CD11blow Ly6Glow cells
CD11b
Ly6G
Neutrophils
MerTK
CD64
Resident macs
Ly6C
CD64
Ly6C
MHCII
Ly6Chi mono
Mo-DC
MHCII
CD11c
cDC
E
Number of cells / mg
8000
6000
4000
2000
0
Day 0
Day 1
Day 2
Day 4
Day 7
Day14
Day 28
Mo-DC
cDC
Ly6Chi mono
Neutrophil
F
CD45.2
CD45.1
Parabiosis
2 wk
CAWS i.p to both mice
2 wk
Analysis
G
Host-derived
Partner-derived
% leukocyte chimerism
80
60
40
20
0
n.s.
n.s.
Blood
Spleen
Heart
Lung
H
Neutrophil
54.0
46.0
cDC
53.6
46.4
Ly6Chi mono
51.0
49.0
Mo-DC
55.9
44.1
CD45.1
CD45.2
I
Host-derived
Partner-derived
% chimerism
80
60
40
20
0
n.s.
n.s.
Neutrophil
cDC
Ly6Chi mono
moDC

Figure 1. CAWS induces inflammatory monocyte recruitment into the heart on day 1. **(A)** Representative H&E–stained horizontal section of the aortic root area from WT naïve mice or on day 28 after 5 daily i.p. injections of CAWS beginning on day 0. Low-power field shows aortic root area and high-power field shows the ostium of the coronary artery within the aortic root. Scale bars= 400 μm. **(B and C)** Coronal section isolated from naive or CAWS-injected WT mice (on day 1, 7 or 28) stained with anti-Ly6G/Ly6C **(B)** or F4/80 **(C)** for IHC. Cropped high-power field images shows aortic root (upper panel) or myocardium (lower panel). Scale bars, 1 mm. **(D)** Representative FACS analysis of heart neutrophil, macrophage, DC and monocyte subsets recovered from CAWS-injected mice on day 1 after the first CAWS injection. One representative of 3 independent experiments. **(E)** Kinetics of absolute cell numbers of the indicated immune cell subset per mg of heart isolated during the course of CAWS-induced vasculitis (mean ± SEM, n=4-5 mice per time point, $p<0.05$, **, $p<0.01$ versus day 0, using unpaired two-tailed Student's t test). **(F)** Schematic protocol for parabiosis experiment. **(G)** Tissue chimerism was analyzed in parabiotic pairs by measuring the frequency of host-derived leukocytes ($CD45.1^+$) and partner-derived leukocytes ($CD45.2^+$) on day 14 after CAWS injection (mean ± SEM, n=4 mice). n.s. means statistically identical in indicated organs among host-derived cells or partner-derived cells using ordinary one-way ANOVA with a post hoc Tukey's test. **(H)** Representative FACS plots of each myeloid cell subset in the parabiotic mouse hearts on day 14 after the 1st CAWS injection. **(I)** Quantitation of chimerism for the indicated myeloid cell subsets (mean ± SEM, n=4 mice). All values were statistically identical in indicated cell subsets among host-derived cells or partner-derived cells using ordinary one-way ANOVA with a post hoc Tukey's test.

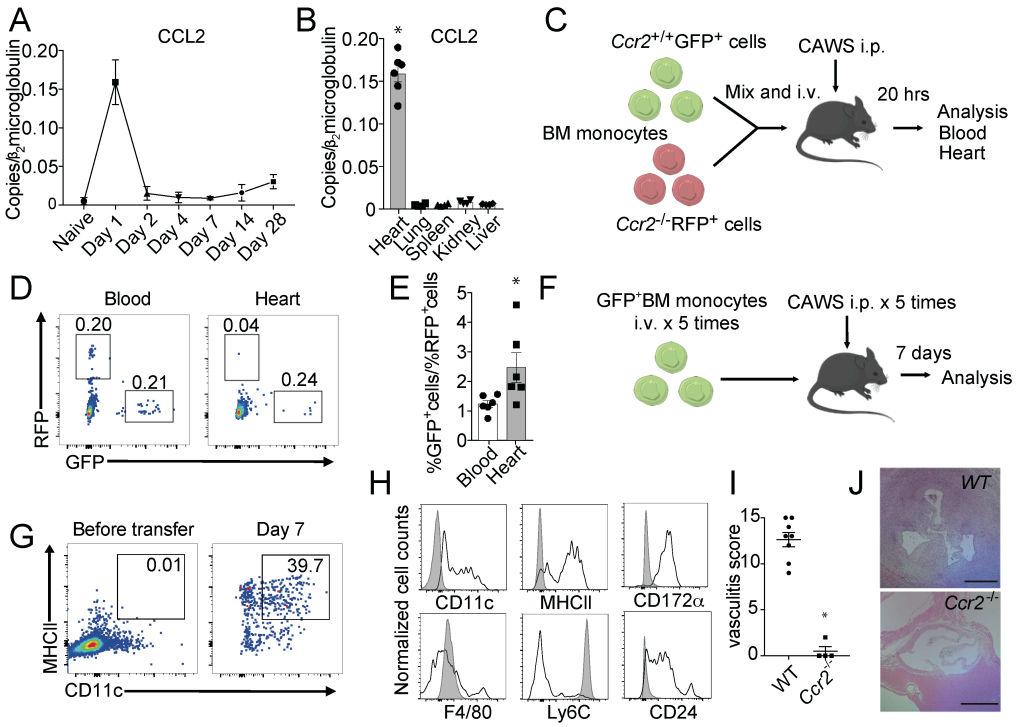

Figure 2. CCL2 is induced in the heart on day 1 and promotes CCR2$^+$ monocyte recruitment. **(A)** Kinetics of CCL2 mRNA expression in the heart following CAWS injection. **(B)** CCL2 expression in various organs on day 1 after CAWS injection (mean ± SEM, n = 4 mice per group, *, p< 0.001 versus lung, spleen, kidney and liver). **(C)** Schematic of co-adoptive transfer of WT and *Ccr2*$^{-/-}$ bone marrow-derived monocytes (BMDM) into WT mice followed by CAWS injection. Equal numbers of *Ccr2*$^{+/+}$GFP$^+$ and *Ccr2*$^{-/-}$RFP$^+$ BMDMs were mixed and intravenously transferred into WT recipient mice along with CAWS injection daily for 5 days. Peripheral blood and heart of recipient mice were analyzed 20h after cell transfer. **(D)** Representative FACS plots of the indicated tissues 20h after adoptive transfer of BMDM and CAWS injection. *Ccr2*$^{+/+}$GFP$^+$ and *Ccr2*$^{-/-}$RFP$^+$ cells in the heart tissue are shown. Numbers indicate percent of live CD45$^+$ cells. **(E)** Ratio of *Ccr2*$^{-/-}$RFP$^+$cells / *Ccr2*$^{+/+}$ GFP$^+$ cells in the indicated tissues (mean ± SEM, n = 6 mice, *, p< 0.05 versus blood). **(F)** Schematic of adoptive transfer of GFP$^+$ BMDM into WT mice followed by CAWS injection. **(G)** Representative FACS plots of the CD45$^+$ GFP$^+$ live BMDM cell population before adoptive transfer and those recovered from the heart 7 days

after CAWS injection. CAWS-injected recipient mice were adoptively transferred with GFP^+ BMDM (once daily for 5 days). **(H)** Representative histograms of the GFP^+ live cell population before adoptive transfer (filled gray) and those recovered from heart 7 days after CAWS injection (black line). **(I)** Histological vasculitis scores were determined in WT and *Ccr2*$^{-/-}$ mice on day 28 (mean ± SEM, *, $p< 0.001$ versus WT). **(J)** H&E stained sections of aortic root lesions from WT and *Ccr2* $^{-/-}$ mice on day 28 after CAWS injection. Scale bars= 400 μm. Data in **(G and H)** are representative of 3 independent experiments. All p values were calculated using unpaired two-tailed Student's t test.

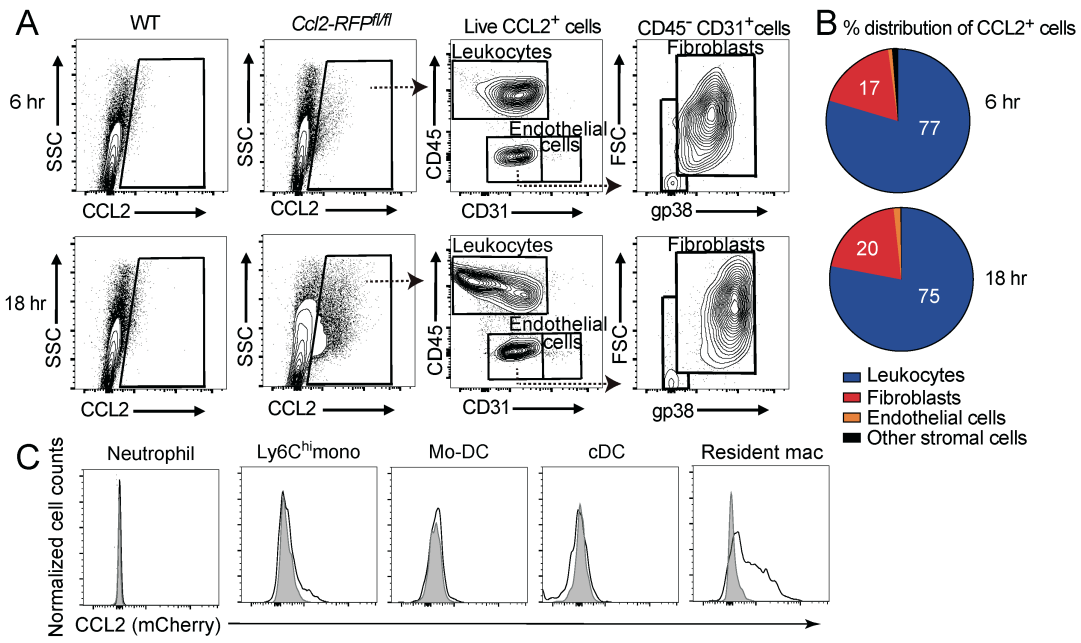

Figure 3. Cardiac resident macrophages are the main source of early CCL2 production. **(A)** Representative contour plots of mCherry^{+} CCL2-expressing cells in live singlets derived from WT or *Ccl2-RFP$^{fl/fl}$* reporter mice heart 6h and 18h after CAWS injection. One representative of 3 independent experiments. **(B)** Pie chart showing percentage distribution of mCherry^{+} cells for the indicated subpopulations in *Ccl2-RFP$^{fl/fl}$* reporter mice heart 6h and 8h after CAWS injection. **(C)** Representative histograms of CCL2 expression in myeloid populations isolated from the hearts of *Ccl2-RFP$^{fl/fl}$* reporter mice day 1 after CAWS injection (n=5 mice). Individual leukocyte populations were immunophenotyped based on the gating strategy shown in **Fig. 1A**. Reporter mCherry was used to identify CCL2-producing cells.

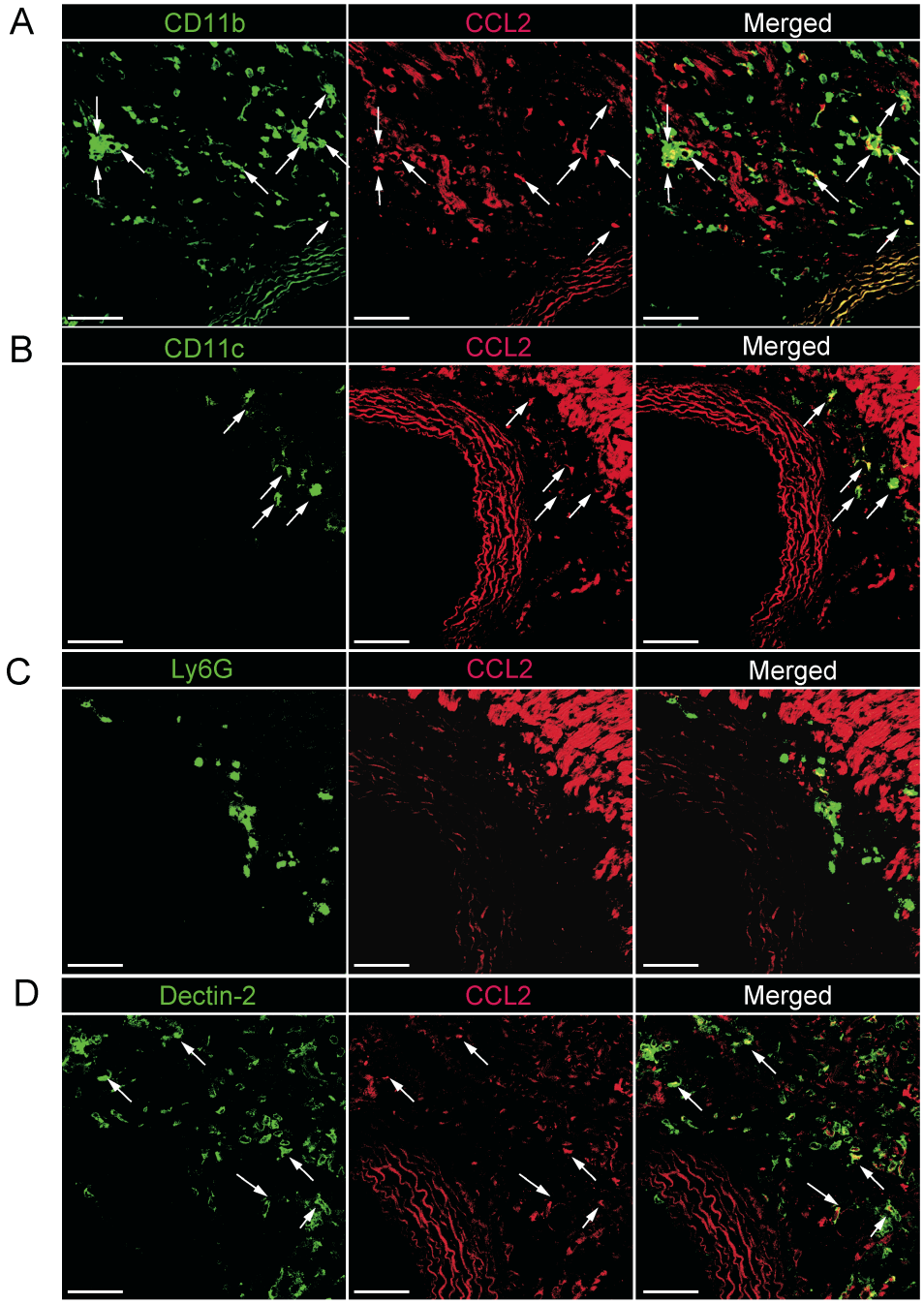

Figure 4. CCL2 is produced by CD11b^{+}Dectin-2^{+} resident cardiac macrophages around the aorta. (A-D) Heart tissue of *Ccl2-RFP$^{fl/fl}$* reporter mice on day 1 after CAWS injection was stained for CD11b **(A)**, CD11c **(B)**, Ly6G **(C)** and Dectin-2 **(D)** (all green) and analyzed by confocal microscopy. Arrows indicate co-localization with CCL2 (red). Scale bars= 40 um.

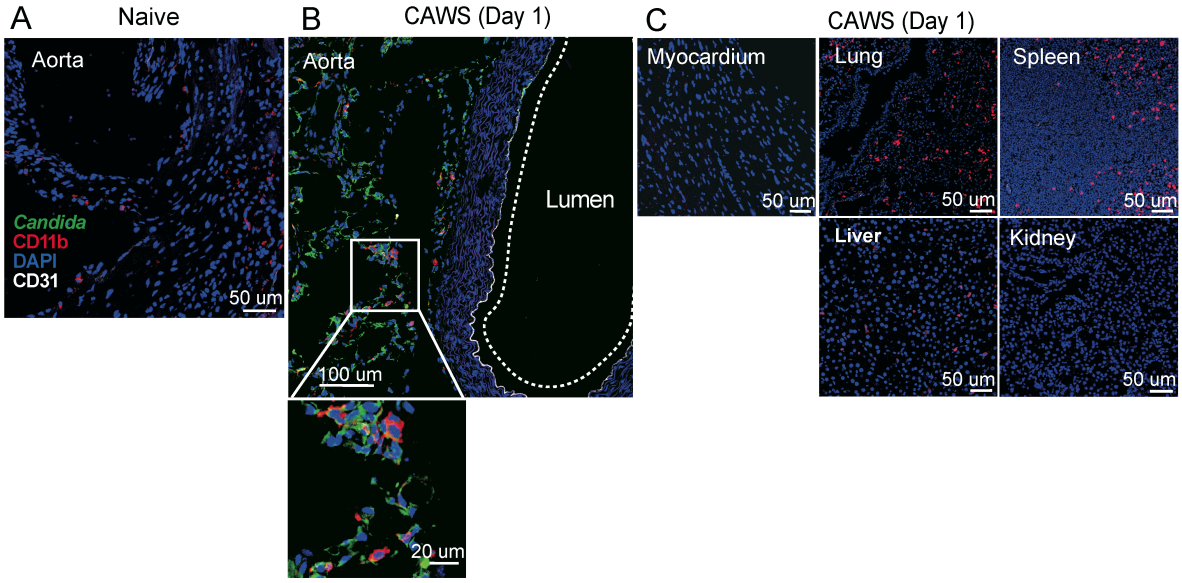

Figure 5. CAWS components are delivered to the aortic root area on day 1 after CAWS injection. Each organ was isolated from naive **(A)** or CAWS-injected WT mice on day 1 **(B and C)** and stained with anti-Candida albicans (green), anti-CD11b (red) and anti-CD31 (white). Representative images of 6 mice from three experiments are shown.

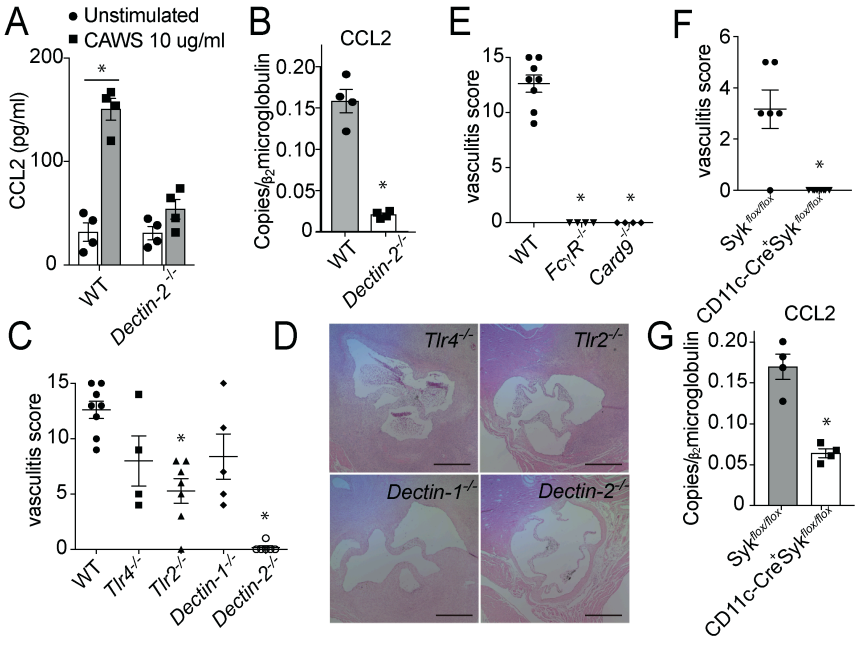

Figure 6. Dectin-2 is required for CAWS-induced CCL2 production and the development of vasculitis. **(A)** F4/80^{+} cells isolated from the heart were stimulated with CAWS (10 ug/ml) for 18h and CCL2 protein in the culture supernatant was measured by ELISA (mean ± SEM from two experiments; *, p=0.001 versus unstimulated). **(B)** Wild type and *Dectin-2*$^{-/-}$ mice were injected with CAWS, and 1 day later hearts were harvested and assessed for *Ccl2* RNA expression by qPCR (mean ± SEM, n= 4 to 6 from two experiments, *, p< 0.0001 versus WT). **(C)** Vasculitis scores of *Tlr4*$^{-/-}$, *Tlr2*$^{-/-}$, *Dectin-1* $^{-/-}$ or *Dectin-2* $^{-/-}$ mice on day 28 after CAWS injection (mean ± SEM, n= 4-8 mice per group, *, p< 0.001 versus WT). **(D)** Hematoxylin and eosin stained aortic root lesions isolated from *Tlr4*$^{-/-}$, *Tlr2* $^{-/-}$, *Dectin-1*$^{-/-}$ or *Dectin-2*$^{-/-}$ mice on day 28. Scale bars= 400 um. **(E)** Vasculitis scores of *FcγR*$^{-/-}$ or *Card9* $^{-/-}$ mice on day 28 after CAWS injection (mean ± SEM, *, p< 0.0001 versus WT). (**F**) Vasculitis scores of CD11cΔSyk mice or control mice (Syk$^{flox/flox}$) on day 28 after CAWS injection (mean ± SEM, *, p< 0.0001 versus Syk$^{flox/flox}$). **(G)** CD11cΔSyk mice or control mice were injected with CAWS, and 1 day later, heart tissues were harvested and assessed for *Ccl2* RNA expression by qPCR (mean ± SEM, n= 4 mice per group, *, p< 0.001 versus Syk$^{flox/flox}$). P values were calculated using unpaired two-tailed Student's t test **(A, B, F and G)** or one-way ANOVA with Dunnett's post-hoc test **(C and E)**.

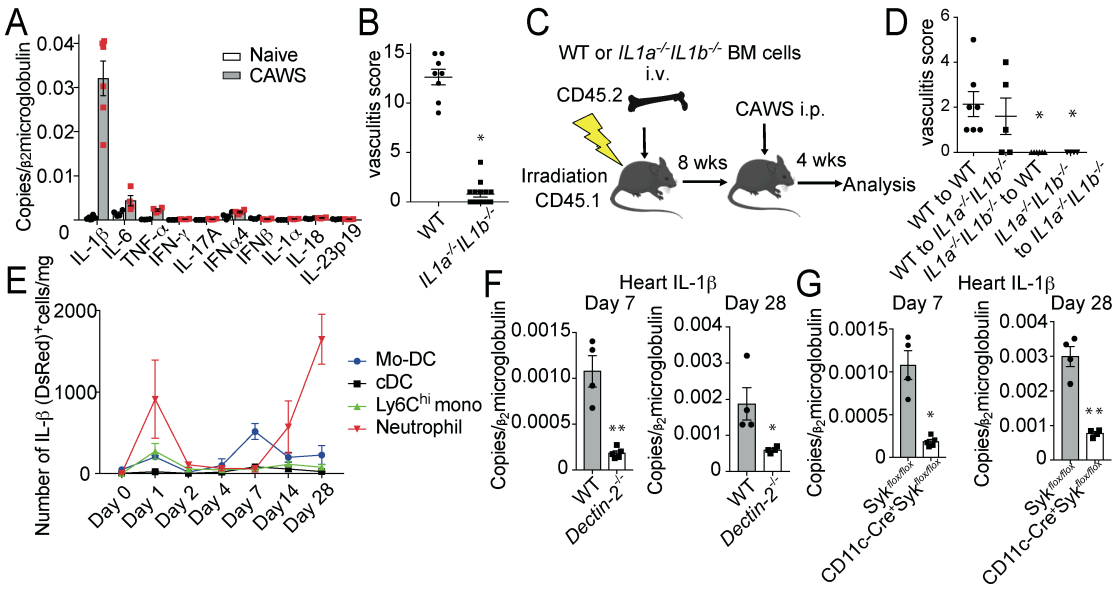

Figure 7. Dectin-2-dependent production of IL-1β from CD11c$^+$ cells is required for CAWS-induced vasculitis. **(A)** Heart tissue from WT mice was harvested 28 days after initial CAWS injection and assessed for cytokine expression by qPCR (n=4-5 per group, mean ± SEM). **(B)** Vasculitis scores of *IL1a$^{-/-}$IL1b$^{-/-}$* mice or WT mice 28 days after CAWS injection (mean ± SEM, *, p< 0.0001 versus WT). **(C)** Schematic of BMC mice generation using WT and *IL1a$^{-/-}$IL1b$^{-/-}$* mice. **(D)** Vasculitis scores were assessed 28 days after CAWS injection into 8-week reconstituted WT → WT, WT → *IL1a$^{-/-}$IL1b$^{-/-}$*, *IL1a$^{-/-}$IL1b$^{-/-}$* → *IL1a$^{-/-}$IL1b$^{-/-}$* and *IL1a$^{-/-}$IL1b$^{-/-}$* → WT BMC mice (mean ± SEM, *, p< 0.01 versus WT to WT). **(E)** Kinetics of IL-1β (DsRed)$^+$ cell numbers of the indicated immune cell subset per mg of heart tissue determined by flow cytometric analysis on day 0, 1, 2, 4, 7, 14 or 28 days after CAWS injection of *pIl1b-DsRed* mice (mean ± SEM, n=3 per time point). **(F)** *Dectin-2 $^{-/-}$* or WT mice were injected with CAWS and 7 or 28 day later hearts were harvested and assessed for IL-1β expression by qPCR (mean ± SEM, n=4-5 per group). **(G)** CD11cΔSyk mice or control mice were injected with CAWS and 7 or 28 day later hearts were harvested and assessed for IL-1β expression by qPCR (**F and G**; mean ± SEM, *, p<0.05, **, p<0.001 versus *Syk$^{flox/flox}$*). P values were calculated using unpaired two-tailed Student's t test **(B, F and G)** or one-way ANOVA with Dunnett's post-hoc test **(D)**.

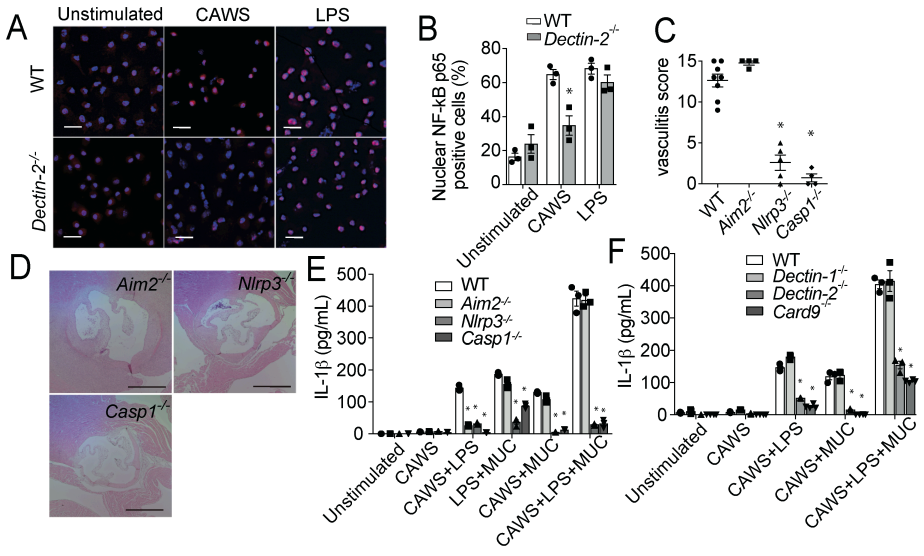

Figure 8. CAWS activates the NLRP3 inflammasome and promotes IL-1β production via Dectin-2. (A) Representative immunofluorescence staining showing NF-kB p65 (red) nuclear translocation in WT and *Dectin-2* $^{-/-}$ BMDM stimulated for 60 mins with CAWS (10 ug/ml) or LPS (1 μg/ml). Cell nuclei were detected by DAPI (blue). Similar results are obtained from three independent experiments. Scale bars: 20 μm. **(B)** Quantitation of NF-kB p65 nuclear translocation in the indicated groups. Results are expressed as the percentage of the p65 nuclei-positively stained cells to the total cells. Similar results are obtained from three independent experiments (mean ± SEM, n=3 per group, *= p< 0.01 versus WT). **(C)** Vasculitis scores of WT, *Aim2* $^{-/-}$, *NLRP3*$^{-/-}$ or *Caspase-1*$^{-/-}$ mice on day 28 after CAWS injection (mean ± SEM, n= 4-8 mice per group, *, p< 0.0001 versus WT). **(D)** Hematoxylin and eosin stained sections of aortic root lesions isolated from *Aim2* $^{-/-}$, *NLRP3*$^{-/-}$ or *Caspase-1*$^{-/-}$ mice on day 28. Scale bars= 400 um. **(E)** BMDCs from WT, *Aim2* $^{-/-}$, *NLRP3*$^{-/-}$ or *Caspase-1*$^{-/-}$ mice were stimulated with CAWS with or without inflammasome stimulators (LPS and MUC) for 18h, and IL-1β release was assessed by ELISA (mean ± SEM, n=3 per group, *, p< 0.0001 versus WT). **(F)** BMDCs from *Dectin-1*$^{-/-}$, *Dectin-2*$^{-/-}$ *or Card9*$^{-/-}$ mice were stimulated with CAWS with or without inflammasome stimulators (LPS and MUC) for 18h, and IL-1β release was assessed by ELISA (mean ± SEM, n=3-4 per group, *, p< 0.0001 versus WT). P values were calculated using unpaired two-tailed Student's t test **(B)** or one-way ANOVA with Dunnett's post-hoc test **(C, E and F)**.

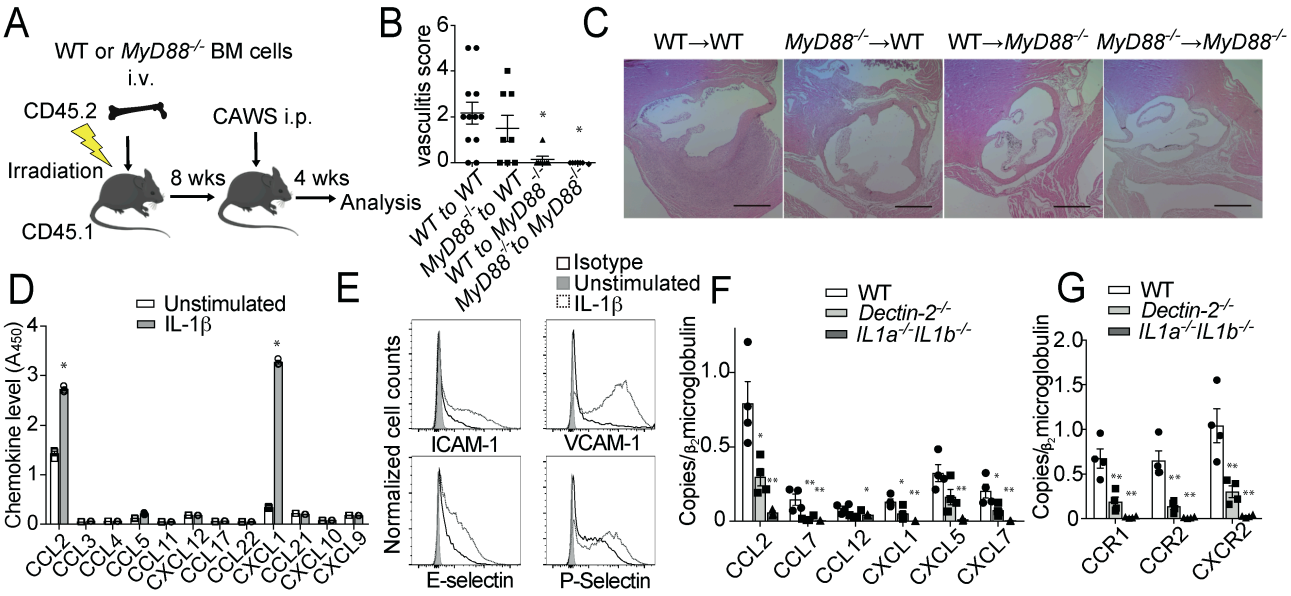

Figure 9. IL-1β-MyD88 signaling in heart stromal cells is required for chemokine and adhesion molecule induction and the development of vasculitis. **(A)** Schematic of BMC mice generation using WT and *MyD88*$^{-/-}$ mice. **(B)** Vasculitis scores were assessed 28 days after CAWS injection into 8 week reconstituted WT → WT or WT → *MyD88*$^{-/-}$ vs. *MyD88*$^{-/-}$→ *MyD88*$^{-/-}$ or *MyD88*$^{-/-}$→ WT BMC mice (mean ± SEM, 7-12 mice per group, *, $p < 0.01$ versus WT). **(C)** H&E staining of aortic root lesions isolated from the indicated BMC mice on day 28. Scale bars= 400 um. **(D and E)** Mouse aortic endothelial cells were stimulated with IL-1β (10 ng/ml) for 18h and chemokine protein levels in the culture supernatant were measured by ELISA (mean ± SEM, n=3, *, $p < 0.0001$ versus Unstimulated) **(D)**. The expression levels of adhesion molecules were assessed by flow cytometry **(E)**. One representative of 3 independent experiments. **(F and G)** qPCR analysis for chemokines **(F)** and chemokine receptors **(G)** in heart tissues isolated from WT, *Dectin-2*$^{-/-}$ or *IL1a*$^{-/-}$*IL1b*$^{-/-}$ mice 28 days after CAWS injection (mean ± SEM, 4-6 mice per group, *, $p < 0.05$ versus WT, **, $p < 0.01$ versus WT). P values were calculated using unpaired two-tailed Student's t test **(D)** or one-way ANOVA with Dunnett's post-hoc test **(B, F and G)**.